Thermal and dynamic mechanical characterization of miscanthus stem fragments: Effects of genotypes, positions along the stem and their relation with biochemical and structural characteristics

Lucie Chupin, Lata Soccalingame, Dieter de Ridder, Emilie Gineau, Gregory Mouille, Stéphanie Arnoult, Maryse Brancourt-Hulmel, Catherine C. Lapierre, Luc Vincent, Alice Mija, et al.

Thermal and dynamic mechanical characterization of miscanthus stem fragments: Effects of genotypes, positions along the stem and their relation with biochemical and structural characteristics

Lucie Chupin[a], Lata Soccalingame[b,1], Dieter de Ridder[a], Emilie Gineau[d], Grégory Mouille[d], Stéphanie Arnoult[e], Maryse Brancourt-Hulmel[f], Catherine Lapierre[d], Luc Vincent[g], Alice Mija[g], Stéphane Corn[c], Nicolas Le Moigne[b,*], Patrick Navard[a,*]

[a] Mines ParisTech, PSL-Research University, CEMEF-Centre de Mise en Forme des Matériaux, UMR CNRS 7635, CS 10207, Rue Claude Daunesse, 06904, Sophia Antipolis Cedex, France[2]
[b] Polymers Composites and Hybrids (PCH) – IMT Mines Ales, Ales, France
[c] LMGC, IMT Mines Ales, Univ Montpellier, CNRS, Ales, France
[d] INRAE, Institut Jean-Pierre Bourgin, UMR1318 INRA-AgroParisTech, ERL3559 CNRS, Saclay Plant Sciences, 78026 Versailles, France
[e] INRAE, UE GCIE, Estrées-Mons, 80203 Péronne, France
[f] BioEcoAgro Joint Research Unit – INRAE – Université de Liège – Université de Lille – Université de Picardie Jules Verne, Site d'Estrées-Mons CS 50136, 80203 Péronne cedex, France
[g] Université Côte d'Azur, Institut de Chimie de Nice (ICN), CNRS UMR 7272, 28, Avenue Valrose, 06108 Nice Cedex 2, France

A B S T R A C T

The thermal and dynamic mechanical properties of miscanthus stem fragments and differences between genotypes and positions along the stem are studied in relation with their biochemical and structural characteristics. The starting degradation temperature does not correlate to the biochemical composition. However, the first DTG peak temperature is negatively correlated to hemicelluloses content and positively correlated to lignin and p-coumaric contents. A pronounced genotypic effect is evidenced on fragments elastic moduli while limited effect of the position along the stem is found. This is mostly related to ferulic and *p*-coumaric acid contents of stem fragments for which a strong correlation to elastic moduli is evidenced. Our results highlight that genotypic effect, position along the stem, stem fragment dimensions and mechanical properties of miscanthus stem fragments are strongly interconnected in relation with their respective biochemical and structural characteristics. This opens interesting perspectives for identifying key biological traits that need to be optimized for a better selection of performing miscanthus genotypes targeted to polymer composite applications.

Keywords:
Miscanthus
Stem fragments
Genotype
Thermal properties
Mechanical properties

1. Introduction

Natural and renewable fillers are more and more popular to manufacture polymer composites and concrete (Vo and Navard, 2016; Girijappa et al., 2019; Onuaguluchi and Banthia, 2016). There are many good reasons for this move. In the polymer composite area, the replacement of heavy glass fibres is an important asset in the transport and sports and leisure industry where weight is a critical issue for performances and energy savings. In the concrete sector, adding biomass brings lightness, good thermal and acoustic insulation, and helps decreasing the environmental footprint of concrete.

There have been numerous trials for preparing composites using a lot of different biomass sources. Recent reviews are summarizing and analysing this body of research (for example in Bourmaud et al., 2018;

* Corresponding authors.
E-mail addresses: lucie.chupin@gmail.com (L. Chupin), lata.soccalingame@univ-ubs.fr (L. Soccalingame), dieter.de.ridder@hotmail.com (D. de Ridder), gineauemilie@gmail.com (E. Gineau), gregory.mouille@inrae.fr (G. Mouille), stephanie.arnoult-carrier@inrae.fr (S. Arnoult), maryse.brancourt@inrae.fr (M. Brancourt-Hulmel), catherine.lapierre@inrae.fr (C. Lapierre), luc.vincent@univ-cotedazur.fr (L. Vincent), alice.mija@univ-cotedazur.fr (A. Mija), stephane.corn@mines-ales.fr (S. Corn), nicolas.le-moigne@mines-ales.fr (N. Le Moigne), patrick.navard@mines-paristech.fr (P. Navard).
[1] Present address: Université Bretagne Sud, IRDL FRE CNRS 3744, 56100 Lorient, France.
[2] Member of the European Polysaccharide Network of Excellence (EPNOE), www.epnoe.eu.

Deyholos and Potter, 2014; Dicker et al., 2014; Ramamoorthy et al., 2015; Thakur et al., 2014). Many plant parts, usually named as "fibres" for composite industry, can be used as reinforcements for polymer composites. These plant fibres should have a high aspect ratio in order to offer the best stress transfer between fillers and matrix, and hence the best mechanical performances of the final products. Plant fibres can be extracted from different plant organs (from leaves as sisal or abaca, or from seeds as cotton), but also from structural tissues of various locations as xylem in wood or outside of xylem within the vascular cambium or procambium for annual plants (case of bast fibres like flax, hemp, or ramie) (Bourmaud et al., 2018). Such fibres are usually long and hence relatively flexible. Some plant fibres can be individual cells (case of cotton) or in the form of cell bundles (flax) or complex tissues (stem fragments) glued with different biopolymers as lignin and pectins. They have a variable content of cellulose that is the primary structural linear polysaccharide found in plants, organized in semi-crystalline oriented microfibrils embedded in a matrix of hemicelluloses and lignin. This complex and hierarchical supramolecular bio-assembly brings stiffness and strength to plants (Mohanty et al., 2005).

The biochemical composition and structural organization of biopolymers within cell walls influence greatly the mechanical properties of elementary fibres and stem fragments. In the case of flax fibres, it has been shown that components contributing the most to the fibre stiffness and strength are firstly cellulose microfibrils, then structuring non-cellulosic components (as pectins and hemicelluloses) interacting with cellulose microfibrils (Alix et al., 2009; Bourmaud et al., 2013; Charlet et al., 2009; Lefeuvre et al., 2015b). Sena Neto et al. (2015) studied the physical properties of different pineapple leaf fibre varieties in relation with their biochemical and structural characteristics. These authors found direct proportional correlations between the cellulose content, the crystallinity index I_c and the resulting stiffness, strength and thermal stability of the pineapple fibres; and suggested that these biochemical and structural parameters can be used as selection criteria among the different pineapple leaf fibre varieties. Besides, it was reported for numerous lignocellulosic fibres that their mechanical properties are partly determined by the crystalline organization of cellulose, i.e. the crystallinity index and the microfibrillar angle (Bledzki and Gassan, 1999). At the level of stem sections, other research works showed a strong correlation between the elastic modulus of miscanthus and wheat stem sections and the cellulose and lignin contents as well as their histological features (Kaack et al., 2003; Kong et al., 2013).

Several mechanical and chemical steps are usually needed to achieve the extraction of high-quality fibres. When breaking the whole stem or leaf, the resulting fragments basically consist in bundles of cells that can originate from different plant tissues having various shapes, with a low aspect ratio as in wood or with a slightly higher aspect ratio as in miscanthus. The benefit of using miscanthus stem fragments is that no chemical input is needed for the crops that produce these bio-based fillers, contrary to flax, for example (Dhirhi et al., 2015). When processed with polymers to prepare composites, they can also be more easily dosed by feeding systems and incorporated into polymer melts than long flexible fibres that tend to entangle (Pickering, 2008). Moreover, their aspect ratio is similar to other plant-based fillers after processing with polymer matrices (Girones et al., 2016) and miscanthus seems to be an interesting choice for preparing polymer composites.

Miscanthus is a perennial grass with a high growth rate, high yield per unit area and low input requirements, and has several potential applications (Danalatos et al., 2007; Lewandowski et al., 2003). In Europe, the cultivation of miscanthus is mainly based on a single clone of one species, *Miscanthus x giganteus*, which can be risky in case of pest or disease pressure (Clifton-Brown et al., 2019). However, the varietal offer can be enlarged as twelve to twenty species of miscanthus can be found worldwide (Clifton-Brown et al., 2008).

Several research studies have also been carried out on using this plant as reinforcement in polymer composites with different polymer matrices. Bourmaud and Pimbert (2008) studied polypropylene PP and polylactide PLA composites reinforced by miscanthus stem fragments. The authors reached different conclusions, on one hand that the poor length and aspect ratio of the miscanthus fragments brought to consider them as fillers rather than reinforcing agents. However, they also showed that PLA/ or PP/miscanthus composites have properties in the same range as the most common plant fibres reinforced composites currently used. In particular, they suggest that a compound made of 65 $\%_w$ PP, 5$\%_w$ PP-g-MA (maleic anhydride-grafted polypropylene and 30 $\%_w$ miscanthus is a promising composite material because it has a modulus over 2700 MPa, a strength of 29.6 MPa at yield and an elongation at break of 4%. In another study, Johnson et al. (2005) incorporated miscanthus stem fragments (called fibres) into a starch-based polymer (Mater-Bi from Novamont, Italy). The main advantage of the incorporation of miscanthus into this polymer is an increase of impact strength, ascribed by the authors to a lack of bonding between miscanthus fibres and matrix and to the friction between matrix and fibres leading to an energy redistribution around the fibres (Canché-Escamilla et al., 2002). Several other studies investigated the use of corona discharge treatment (Ragoubi et al., 2012) to improve interfacial compatibility of miscanthus with PLA and PP (with a limited effect), of a reactive extrusion process (Zhang et al., 2014a) and of a co-injection moulding technique (Zhang et al., 2014b). Composites of poly (butylene succinate) (PBS) and miscanthus fragments (Muthuraj et al., 2015) were successfully prepared by extrusion and injection moulding methods with different loadings. Addition of 5 wt % maleic anhydride grafted PBS (MAH-g-PBS) into PBS composites brought a significant improvement in tensile and flexural strength. Thirteen miscanthus genotypes were compared for their reinforcement capability in polypropylene composites reinforced with stem fragments (Girones et al., 2016). The protocol focused on the use of the whole crop harvest reduced into stem and leave fragments. The preparation contains a matrix of polypropylene reinforced with 30 % w/w content of miscanthus fragments of varying sizes. The study outlines a 17 % variability among genotypes for tensile strength and Young's modulus.

Moving now on the genotype characteristics such as biochemical variables, the smallest units and highest quality cellulose fibres from miscanthus stems were extracted by an alkali-methanol-anthraquinone pulping process of *Miscanthus x giganteus* (Lundquist et al., 2004). With the optimal pulping conditions, cellulose fibres were thermally stable up to 255 °C, with an aspect ratio of 40, a tensile strength of 890 MPa and a Young's modulus of 60 GPa. This is in the range of values obtained for flax fibres, considered as one of the highest quality fibres (Yan et al., 2014). When dealing with the properties of miscanthus stem fragments, i.e. by breaking the whole stem without extracting any component, results are scarce. Using a nanoindentation method to measure the mechanical properties of miscanthus stem fragments, Bourmaud and Pimbert (2008) found a longitudinal modulus of about 10 GPa and a hardness of about 340 MPa, in the same order of magnitude as for hemp, sisal and flax fibres measured by the same methodology. Nevertheless, the authors underlined that the longitudinal moduli of the tested fibres were underestimated because the calculation did not consider the three-dimensional distribution of the stress inherent to the experimental method, and hence the contribution of the transverse modulus. The mechanical properties of full miscanthus stems were studied by Kaack and Schwarz (2001) and Kaack et al. (2003). They cut stem sections of 10 cm length from various places along the stem and correlated their mechanical properties to their position and their biochemical composition and structural organisation. The measured modulus of these stem sections was in the range of 2–10 GPa. It was also found that stem sections cut from the bottom of the stems have higher stiffness than those from the top of the stem. There was a clear relationship between the modulus of elasticity and the area of (parenchyma × cellulose content), the area of (lignified outer ring × lignin content) and the area of (vascular bundles × cellulose). The authors assumed that the modulus of elasticity of the stem is correlated with both cellulose content and the presence of highly lignified cell walls

that should provide higher lodging resistance to the plants. Although they did not study the incorporation of these stems into composites, these results highlight interesting properties related to biochemical characteristics.

The thermal stability of plants is also known to be very dependent on their biochemical composition. For miscanthus, the thermal degradation of several genotypes was studied in an inert atmosphere, with Heo et al. (2010) and Bok et al. (2013) studying *Miscanthus sinensis var purpurescens* and *sinensis*, respectively. From the derivative thermogravimetric (DTG) curves, two degradation peaks were found at 260 – 290 °C and 335 – 345 °C corresponding to the degradation of hemicelluloses and cellulose, respectively. Kim et al. (2014) worked on *Miscanthus sacchariflorus*, where the DTG curve presented one main degradation peak with a shoulder at 300 °C corresponding to the decomposition of hemicelluloses. *Miscanthus giganteus* was studied by Cortés and Bridgwater (2015) and a single DTG peak was found at 337 °C at 10 °C/min heating rate. Due to its specific molecular structure, lignin often degrades over a wide range of temperature (Benítez-Guerrero et al., 2014) which makes it less discernible. Thermal degradation is also greatly influenced by the preparation and heating parameters (Szabo et al., 1996; Cortés and Bridgwater, 2015). Cortés and Bridgwater (2015) varied the heating rate from 2.5 °C/min to 25 °C/min, which led to a positive shifting of the decomposition temperatures of about 50 °C.

To improve crops for any application, and in particular for a material type application such as natural fibres reinforced polymer composites, plants must be optimized at several levels by selecting the best genotype, the best cultivation and harvesting methods, the best milling and compounding conditions and the best composite processing. The present work is primarily targeting the first level, genotype effect and traits being of great importance for breeding purposes. For such industrial uses, we hypothesized that the miscanthus genotypic effect may be related to biochemical characteristics. We also hypothesized that the composition of the stem is not homogeneous along the stem and that may vary between the genotypes. Lastly, the fragmentation processes may interfere with the biochemical characteristics and mechanical properties of the genotypes. Stem fragments of different sizes can be different in composition and histological structures. A variation of composition with plant stem fragment sizes, even between two different sieve sizes, was already reported (Vo et al., 2017).

To investigate this, we performed detailed studies relating several genotype characteristics, here biochemical, with several physical properties relevant to composite preparation, here thermal stability and mechanical characteristics of stem fragments. To be able to clearly relate these parameters, their position along the stem must be considered since it can modify their biochemical and structural characteristics. Although it is impossible to select upper or lower parts of stems in an industrial harvesting, this is needed when willing to make very precise correlations between composition and heat stability or mechanical properties of stem fragments. In this regard, specific plant parts were selected in order to be able to well compare the different genotypes.

The present study was thus conducted on miscanthus stem fragments ground from lower and upper parts of six different miscanthus genotypes. Their biochemical composition, crystallinity index, thermal stability and mechanical properties were measured and discussed in relation with the testing conditions. These genotypic-related data and correlations will be a useful tool to identify the biological traits that will need to be optimized for composite applications and to guide selection and breeding.

2. Materials and methods

2.1. Sampling of miscanthus genotypes and preparation of stem fragments

Six clones of miscanthus were planted in 2007, according to a three randomised complete block design, in the Picardie region of Northern France (49°53 N, 3°00E) at the INRAE experimental unit in Estrées-Mons. Two clones were *M. x giganteus* clones: the variety Floridulus (FLO) and a clone from the Agriculture Development and Advisory Service in Great Britain (GIGB). Two clones were identified as *M. sinensis* clones: Goliath (GOL) and Malepartus (MAL). Finally, two clones were identified as *M. sacchariflorus* clones: one hybrid (H5) from the Danish Aarhus University and one clone from Chombard nursery (SAC). The plant density was two plants per m^2. No irrigation was applied except during the first year of cultivation. No inputs were applied during the entire plantation time and, in order to preserve the quality of the crop for industrial testing and genotype comparisons, the weeds were controlled during the two first years by hand and machine hoeing. The plants were harvested at the end of winter at over-maturity in 2014, which corresponded to a mature crop of seven years old. Two positions along the stem were selected. The upper (U) position and the lower (L) position corresponded to the second internode from the top or from the bottom of the stem, respectively.

The leaves from collected upper and lower stem sections of each genotype were removed and stems were first manually cut into small pieces of a few centimeters with scissors. These stem pieces were then ground with a polymer pelletizer (Hellweg M50) equipped with a 2.5 mm sieve. Further grinding was done with a coffee mill (Carrefour home) for 30 s. Based on these ground fractions, two different genotype samplings were prepared to characterize stem fragments:

- In genotype sampling A gathering all genotypes, about 20 g of each were sieved using a Retsch AS200 Digit shaker (Retsch, Germany) operating at 40 mm amplitude for 5 min. Three fractions, between 200 and 300 µm, between 100 and 200 µm and smaller than 100 µm, were collected. This sieving method, used for preparing composites, is different from what is occurring in industry. As explained in Girones et al. (2016), such robust method ensures a very strong reproducibility of the experiments and is essential to compare genotypes.
- In genotype sampling B, regular and slender stem fragments of lower (L) and upper (U) parts of only three genotypes (FLO, GIGB and GOL) were selected and collected manually from the ground fractions before sieving (Fig. 1-a). Only these three genotypes were giving after breaking large amounts of stem fragments suitable for being studied in the mechanical testing set-up, i.e. having a regular shape all along their length. We do not know why it was not possible

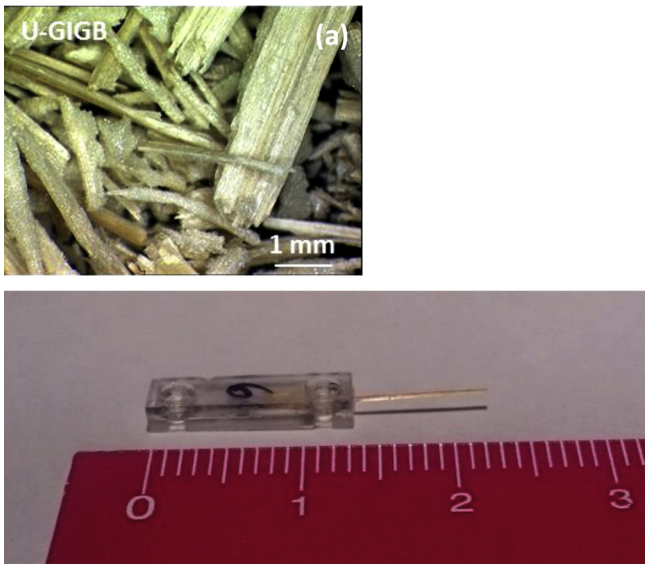

Fig. 1. Sampling B. (a) Ground fraction of a lower part of GIGB, (b) a selected stem fragment from the ground fraction set up as a cantilever beam and clamped between two plastic tabs.

to have long and regular fragments with the other genotypes. The selected samples are bundles composed of numerous elementary plant cells. 20–30 of such stem fragment samples were collected and tested for each of the three studied genotypes at upper (U) and lower (L) positions along the stem. As seen on Fig. 1-b, each selected stem fragment was positioned like a cantilever beam, then stuck and clamped between two plastic tabs at one extremity.

It must be remembered all along the paper that there is a difference in these two procedures of fragment sampling. The fragments are different in size and shape, and hence can be different in terms of composition and histological structures. The reason for these two samplings is as follows. If willing to have information on miscanthus fragments of sizes used for preparing composite materials, the size must be below 1 mm, but if the targeted information are the mechanical properties of the stem fragments, the size must be above 5 mm for experimental reasons.

The sieved fractions of all genotypes obtained from sampling A will be used for biochemical composition and thermogravimetric analysis. Ground fractions from sampling B will be used for X-ray scattering and density measurements. Regular stem fragments selected from ground fractions of sampling B will be used for local biochemical analysis and mechanical characterisation.

2.2. Biochemical composition of miscanthus stem fragments

The biochemical compositions of the selected upper (U) and lower (L) stem parts of genotype sampling A were measured with the following procedures.

Monosaccharide composition of polysaccharides: the analyses of polysaccharides were performed on an alcohol insoluble material prepared as follows. 100 mg of materials were washed four times in 4 volumes of absolute ethanol for 15 min at 80 °C, then rinsed twice in 4 volumes of acetone at room temperature for 10 min and left to dry under a fume hood overnight at room temperature. Neutral monosaccharide composition was performed on 10 mg of dried alcohol insoluble material after hydrolysis in 2.5 M trifluoroacetic acid for 2 h at 100 °C as described respectively in (Harholt et al., 2006). To determine the cellulose content, the residual pellet obtained after the monosaccharide analysis was rinsed twice with ten volumes of ethanol and once with 10 volumes of acetone and hydrolysed with H_2SO_4 as described in (Updegraff, 1969). The released monosaccharides of hemicellulose were diluted 500 times and the released glucose of cellulose was diluted 1000 times. Then the monosaccharides were quantified using an HPAEC-PAD chromatography as described in (Harholt et al., 2006).

Lignin amount was estimated using the Acetyl Bromide Lignin (ABL) method and from extract-free sample, as follows: 100 mg of dry ground sample were washed twice in 3 mL of water at 80 °C for 15 min, twice in 3 mL of ethanol at 80 °C for 15 min and twice in 3 mL acetone at room temperature for 10 min and left to dry under a fume hood overnight at room temperature. The amount of ABL was measured from about 10 mg of extract-free sample (weighted to the nearest 0.1 mg) according to a procedure adapted from Fukushima and Hatfield (2001) and described in (Sibout et al., 2016). The ABL lignin content was calculated using the lignin extinction coefficient 20 g L^{-1} cm^{-1} at 280 nm. The amount of ester-linked *p*-coumaric acid (CA) and ferulic acid (FA) was measured by mild alkaline hydrolysis of extract-free sample (about 10 mg weighted to the nearest 0.1 mg) as previously described (Sibout et al., 2016).

Results are given in Table 1S (see supplemental file) for the six selected genotypes. However, even if the sieved fractions (sampling A) were in rather small quantities, it is never sure that the composition and structure of the stem fragments selected for the mechanical tests (sampling B) have the same mean composition as the one of sampling A. Chemical characterisation was thus also performed on the exact stem fragments used for the mechanical testing. The local biochemical composition of the mechanically tested stem fragments (sampling B) is given in Table 2S (see supplemental file).

2.3. Crystallinity index of miscanthus stem fragments

Wide-angle X-ray diffraction (WAXD) was used to determine the crystallinity index of miscanthus stem fragments using an AXS D8 Advance apparatus (Bruker, Germany). Ground fractions of miscanthus fragments (sampling B) were compressed at 20 bars during 5 min at ambient temperature to obtain flat discs of 2 mm thickness. The measurements were carried out at 30 kV and 40 mA and from 5° to 65° (Bragg angles, 2Θ). Several methods have been developed to determine the crystallinity index of cellulosic substrates. The amorphous subtraction method consists in determining the contribution of the crystalline phase on the total diffractogram so as to calculate the crystallinity index *%Ic*. This method was outlined by Ruland and later on by Vonk (Ruland, 1961; Vonk, 1973). The contribution of the non-crystalline (amorphous) fraction is obtained by measuring the scattering of the same cellulosic substrate in the amorphous state. The amorphous state is defined such that the material does not give any indication of the lattice planes in the X-ray diffraction pattern. Amorphous cellulose obtained by ball milling is often used to subtract the non-crystalline contribution from the diffraction profiles (Terinte et al., 2011). The Hermans-Weidinger method is based on the same principle but differs by specific background corrections (air, thermal agitation of the atoms, Compton radiation) (Hermans and Weidinger, 1961). In this study, the crystallinity index *%Ic* was calculated based on the respective contributions of the amorphous halo and crystalline peaks on the diffractograms of miscanthus stem fragments. The amorphous contribution was assessed by fitting arbitrary a broad peak centred at 2θ = 18°. This fitted broad peak was then subtracted from the total diffractogram area between 10° and 30° (2θ) so as to determine the area corresponding to the crystalline contribution. Therefore, the crystallinity index *%Ic* was calculated with the relation:

$$\%Ic = \frac{A_{cr}}{A_{cr} + A_{non-cr}} \times 100 \quad (1)$$

where A_{cr} is the area of the crystalline peaks and $A_{non\text{-}cr}$ is the area of the amorphous halo. Thus, $A_{cr} + A_{non\text{-}cr}$ is the sum of the integrated area of the crystalline and amorphous contributions and equals to the total area of the diffractogram between 10° and 30° (2θ). Three replicates were performed for each sample type. The crystallinity index was estimated for stem fragments of sampling B, FLO, GIGB and GOL, from the lower and upper parts (Table 1). With a standard deviation of about 2% for each fragment type, no significant discrepancies of the crystallinity index can be observed when comparing genotypes at the same position

Table 1
Sampling B. Crystallinity index *%Ic* determined by WAXD on ground fractions of miscanthus stem fragments.

		Lower parts			Upper parts		
		FLO-L	GIGB-L	GOL-L	FLO-U	GIGB-U	GOL-U
Cellulose crystallinity index %Ic	Mean	57.8 %	59.3 %	60.4 %	61.1 %	62.6 %	61.5 %
	Standard deviation	2.2 %	2.6 %	2.0 %	2.4 %	2.0 %	2.3 %

(a)

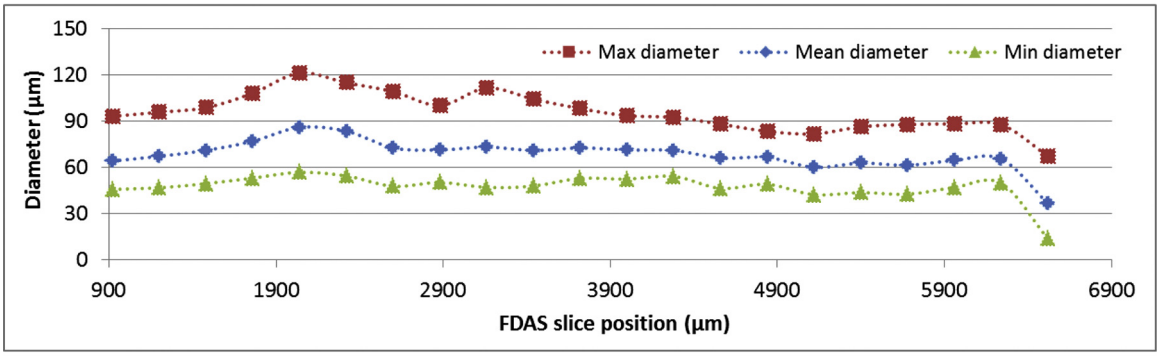

(b)

Fig. 2. Sampling B. Dimensional analysis of a stem fragment sample: (a) length measurement by optical microscopy (L = 7.331 mm) and, (b) minimum, mean and maximum diameters measured along its length on 21 slices with a pitch of 280 µm.

along the stem. In contrast, slightly higher crystallinity indexes are measured for upper parts as compared to lower parts whatever the genotype.

2.4. Thermogravimetric analysis on miscanthus stem fragments

The thermal stability of all six miscanthus genotypes (genotype sampling A) was studied by thermogravimetric analysis (TGA) on a TGA/DSC 1 STARE (Mettler Toledo). First, the influence of the experimental testing conditions was analysed on the upper (U) and lower (L) parts of one genotype, FLO. Not all genotypes were used for both upper and lower parts, but it allows a comparison of the thermal behaviour with composition. The samples were analysed under air atmosphere from 25 °C to 400 °C at a heating rate of 10 °C/min and from 400 °C to 800 °C at 50 °C/min. The effect of particle size and mass of the samples, the air flow and the heating rate between 200 °C and 400 °C were investigated. 10 mg of the three particle sizes (sampling A) were tested (smaller than 100 µm, between 100 and 200 µm and between 200 and 300 µm) with an air flow of 50 mL/min. For a particle size between 100 and 200 µm, samples of 5 mg, 10 mg and 15 mg were analysed with an air flow of 50 mL/min. Then 10 mg of samples with a particle size between 100 and 200 µm were analysed with an air flow of 50 mL/min, 100 mL/min and 150 mL/min. Finally, the heating rate between 200 °C and 400 °C was set at 5 °C/min, 10 °C/min and 20 °C/min for 10 mg of samples with a particle size between 100 and 200 µm and an air flow of 50 mL/min. Based on these experiments, the upper and lower parts were compared for the six different miscanthus genotypes. The samples were heated under air (50 mL/min) from 25 °C to 400 °C at 10 °C/min and from 400 °C to 800 °C at 50 °C/min with a sample mass of 10 mg and a particle size between 100 and 200 µm. The results were analysed with the STARe software. Thermal stability experiments were conducted on two replicates. Standard deviation was less than 3%.

2.5. Dynamic mechanical analysis on miscanthus stem fragments

2.5.1. Vibration frequency measurements

To determine the elastic modulus of selected stem fragments (genotype sampling B), a non-destructive testing method based on the measurement of vibration resonant frequencies was used (Corn et al., 2012). The protocol was the following: the stem fragment is positioned like a cantilever beam (Fig. 1-b) and a brief transverse impulse force is applied at its free end (using a small rigid metal stick) under controlled environmental conditions (23 ± 1 °C and 50 ± 5 % RH). The transient dynamic response of the stem fragment is measured by a mono-point laser displacement sensor (Sunx-Panasonic HL-C2, 100 kHz sampling speed, 0.025 µm resolution). This signal goes through a signal conditioner and is then picked up by an acquisition card (NI-4552) to PC running Labview software. Measured response signals are transformed in frequency spectrum using Fast Fourier Transform. It is then possible to determine the natural frequency of the vibrating stem from the main peak of the frequency spectrum. The elastic modulus E of a cantilever cylinder with elliptical cross-section can be related to its first flexural natural frequency f with Eq. (2), derived from the Euler-Bernoulli's formula:

$$E = C\,\rho_{app}\,\frac{L^4}{{d_{min}}^2} f^2 \ (\text{with } C = 51095\ \text{kg. m}^{-3}) \tag{2}$$

where ρ_{app} is the apparent density, L the length of the beam, d_{min} the minor diameter of the cross-section and C is a theoretical constant that comes from the lowest root of the equation associated to the cantilever boundary conditions (Corn et al., 2013). Some assumptions on the geometry and material microstructure must be considered to use Eq. (2) since the beam theory is only fully valid if the beam is straight, slender, with uniform cross-section, and the material is elastic, homogeneous and isotropic in its cross-section. Upon these assumptions, Eq. 2 allows determining the elastic modulus of a vibrating stem fragment from the measurements of its natural frequency, dimensions, and apparent density. Results are based on the measurements performed on 20–30 stem fragments for each genotype and position along the stem (selected from sampling B).

2.5.2. Length measurement

The length of each stem fragment was measured using an optical microscope (Laborlux 12 POL S) in reflexion mode with a normalized X–Y stage and a high-resolution mono-CCD numerical camera (1600 × 1200 pixels) Sony progressiv scan. In order to enlarge the zone of observation and thus improve the accuracy of the results, high resolution cartographies (0.7 µm per pixel) of the entire stem fragments were built (Fig. 2a) using Archimed software (Microvision Instruments). Based on these cartographies made of 8–20 pictures, the lengths of stem fragments were determined by a digital calliper associated to the software. Length of stem fragments ranged from 3 to 11 mm.

2.5.3. Diameter measurement of cross-section

Each sample was scanned by a laser micrometry method using a FDAS 770 apparatus (Dia-Stron Ltd) and a laser scan micrometer LSM-500/LSM-6200 (Mitutoyo) so as to determine its median diameter. The apparatus spins the sample on 360° and measures diameters (about 600 values per cross-section) along the fibre with a pitch fixed at 280 µm. Thereby, the median apparent diameter of 10–30 cross sections per stem fragment sample were measured. The analysis of the diameter along the length of stem fragments clearly showed that each cross-section exhibits a minor and major diameter (Fig. 2b). Therefore, stem fragments were considered as elliptical cylinders with d being the minor diameter of the ellipse. As the minor diameter (plotted in triangle dots on Fig. 2b) of stem fragments can vary significantly along their length, the median value of the minor diameters was used as the diameter d_{min} for modulus calculation (Eq. 2). Median minor diameters of stem fragments ranged from 30 to 370 µm.

2.5.4. Apparent density measurement

The apparent density ρ_{app} was calculated by determining the specific density and the porosity volume of ground fractions of miscanthus fragments (sampling B) based on Eq. (3):

$$V_p = \frac{1}{\rho_{app}} - \frac{1}{\rho_{spe}} \quad (3)$$

where V_p is the porosity volume per gram of sample, ρ_{app} the apparent density and ρ_{spe} the specific density. ρ_{spe} was measured by helium pycnometry using an AccuPyc 1330 from Micromeritics. Experiments were done at least in triplicate for each genotype and position along the stem, and standard deviation on specific density was about 0.006 g.cm^{-3}.

V_p was estimated by mercury porosimetry using an AutoPore IV 9500 by Micromeritics in the pressure range 0.003 MPa to 207 MPa. This method consists in measuring the volume of mercury introduced at given pressures, and allows determining the pore size distribution and the overall porosity of solid samples, based on the Washburn equation (Giesche, 2006):

$$D = -\frac{4\gamma\cos\theta}{P} \quad (4)$$

where D is the pore diameter, γ the mercury surface tension (485 mJ.m^{-2}), θ the mercury contact angle with any solid material (140°) and P the pressure. Thus, mercury intrusion at low pressure corresponds to the filling of large pores whereas high pressure corresponds to the filling of small pores. According to scanning electron microscopy (SEM) observations, the larger pores in miscanthus stem fragments are the cell lumens. Their diameter was estimated at a mean value of 15 µm. Based on Eq. (4), the volume of mercury intruded into the sample at pressures below 0.1 MPa corresponds to the filling of voids larger than 15 µm, and is thus considered as the free inter-particle volume. On the other hand, the volume of intruded mercury between 0.1 MPa and 207 MPa is considered to be the porosity volume of the tested stem fragments V_p. For both helium pycnometry and mercury porosimetry experiments, ground fractions of stem fragments (sampling B) were collected and stored at 23 ± 1 °C and 50 ± 5 % RH before testing. 200 mg–400 mg of fragments from upper and lower parts of each genotype were tested. The quantity of closed porosity is assumed to be negligible. Resulting values of ρ_{spe}, ρ_{app} *and* V_p are reported in Table 2 for upper and lower parts of each genotype (sampling B). Densities of stem fragments showed that there was no effect of genotype while fragments originating from the lower parts of the stems had higher specific densities.

2.6. Statistical analysis and plots

The experimental design allowed to test factors two by two and the interactions between these two factors were detected using ANOVA according to the following model:

$$Yijk = \mu + \alpha\, i + \beta\, j + REPk + \gamma ij + \varepsilon ijk \quad (5)$$

where Yijk is the value of the trait (for example Cell-Wall) for the first factor i (for example Internode position) according to second factor j (for example Genotype) and replicate (REP) k, μ is the grand mean, αi is the main effect of the first factor i, βj is the main effect of the second factor j, *REP*k is the effect of replicate k, γij is the interaction between the first factor i and the second factor j, and εijk is the residual error term. All models were tested with R (3.6.2 version) using the aov function of agricolae package (1.3–2 version) and means were compared using the Student-Newman-Keuls (SNK) test. A Pearson correlation matrix was calculated and designed using the corrplot function of the corrplot package (0.84 version). For all statistical tests, the α probability level was considered at 0.05. Finally, a collection of boxplots was produced with R using the ggplot function of ggplot2 package.

Table 2
Sampling B. Specific density ρ_{spe}, apparent density ρ_{app} and porosity volume V_p of ground fractions of miscanthus stem fragments.

	Lower parts			Upper parts		
	FLO-L	GIGB-L	GOL-L	FLO-U	GIGB-U	GOL-U
Specific density ρ_{spe} (g. cm^{-3})	1.157	1.125	1.172	1.027	1.089	1.039
Apparent density ρ_{app} (g. cm^{-3})	0.630	0.637	0.665	0.530	0.455	0.443
Volume porosity Vp (cm^3. g^{-1})	0.724	0.680	0.650	0.911	1.280	1.296

3. Results and discussion

3.1. Thermal analysis (TGA) on miscanthus stem fragments

The thermal analysis was performed using miscanthus stem fragments from sampling A. Three main mass loss steps were found for all genotypes (Fig. 3). The first mass loss, up to 120 °C, corresponded to the evaporation of the residual water in the samples. In this study, the starting degradation temperature was defined as the temperature at which 1% mass loss occurs from the mass at 130 °C. The second mass loss occurred from 180 °C to 360 °C, corresponding to the depolymerisation and decomposition by oxidative pyrolysis of the main components of the stem fragments, i.e. cellulose, hemicellulose, lignin and

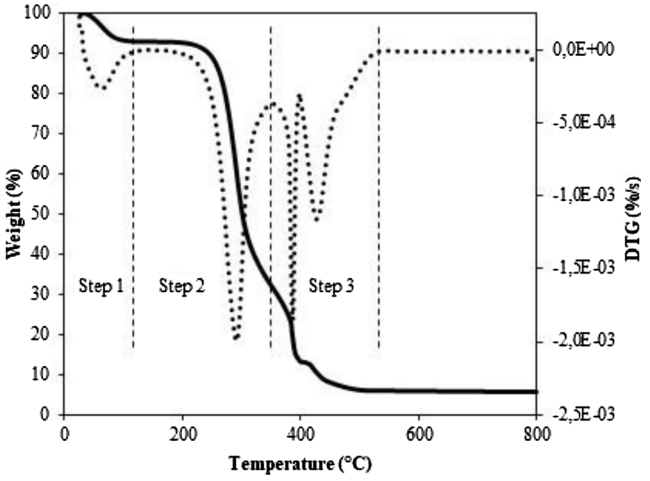

Fig. 3. Sampling A. Typical thermogravimetry (solid line) and differential thermogravimetry curves (dotted line) of a sample of miscanthus stem fragments.

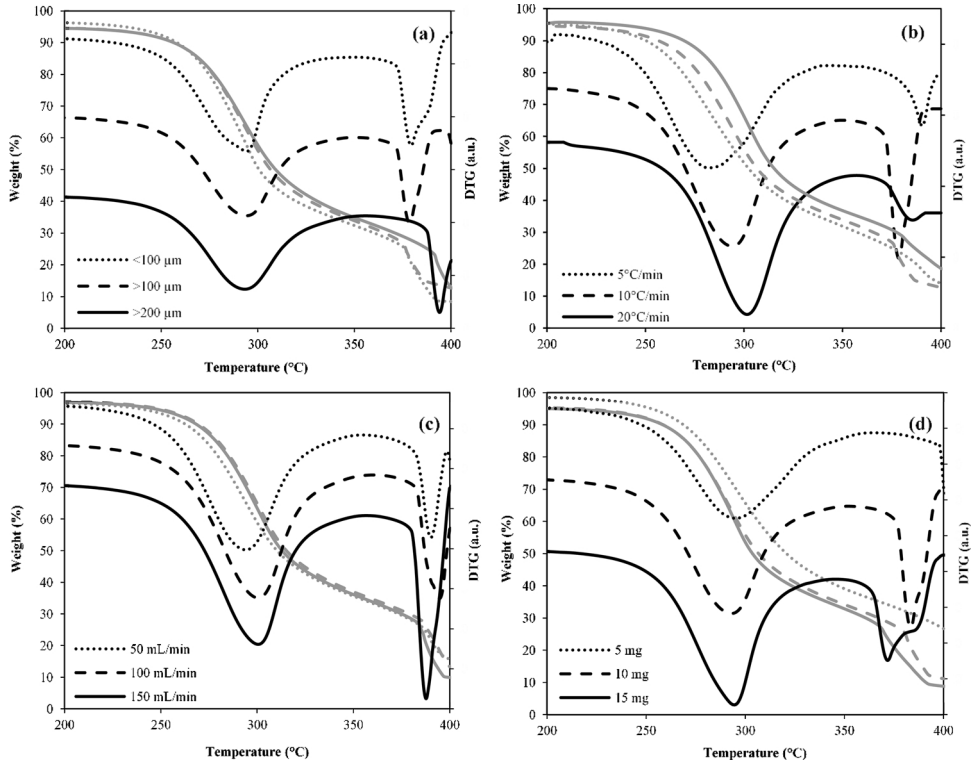

Fig. 4. Sampling A. TG (grey) and DTG (black) curves of the upper part of FLO for: (a) three diameter sizes; (b) three heating rates; (c) three air flows; (d) three sample weights.

other non-cellulosic components. The last mass loss occurs between 360 and 540 °C, and corresponds to the thermal degradation of aromatic rings of lignin and of the residue formed during the first degradation step (Shafizadeh et al., 1972; Tejado et al., 2007; Benítez-Guerrero et al., 2014). Based on these observations, the influence of the TGA testing conditions was firstly investigated.

3.1.1. *Influence of the testing conditions*

The effects of stem fragment size, heating rate, air flow and sample amount were thoroughly analysed on the upper and lower parts of FLO and SAC genotypes.

3.1.1.1. Effect of stem fragment size. The derivative thermogravimetric (DTG) curves of FLO-U for the different particle sizes are presented in Fig. 4-a. Both lower and upper parts, FLO-U and FLO-L, showed the same general behaviour when the size of the stem fragments changed. The fragment size had an effect on the degradation temperature, the mass loss and the mass loss rate. Fragments started to degrade at a higher temperature and they tended to degrade slower when their size increases. A reason can be the kinetics of degradation propagation which should depend on the size of fragments, and induced thermal gradients. Another possible reason, according to Barneto et al. (2011) who found similar results for flax fibres and flax pulps of different sizes, is the variations of the chemical composition and the crystallinity of the fibres as a function of sizes. Indeed, they found that longer fibres have less hemicellulose and lignin than short fibres. The long fibres are also more crystalline than short fibres. A similar influence of the size of sorghum stem fragments on their chemical composition was also found (Vo et al., 2017). Besides, it was found that the mass loss between 180 and 360 °C increases when the stem fragment size decreases. This could be due to the greater amount of dust present in smaller size fractions, which are less thermally stable.

3.1.1.2. Effect of heating rate. The DTG curves between 200 and 400 °C of FLO-U for the different heating rates are presented in Fig. 4-b (FLO-L and SAC-L showed the same behaviour with the heating rate). The starting degradation temperature and the temperature of the DTG peaks were higher when the heating rate increases. The maximum mass loss rate increased when the heating rate increased. Similar results were found for miscanthus, microcrystalline cellulose and xylan-based hemicellulose (Cortés and Bridgwater, 2015; Shen and Gu, 2009; Shen et al., 2010). Heat and mass transfer limitations are responsible for thermal gradients inside the stem fragments which results in a shift of the degradation process to higher temperatures for higher heating rates.

3.1.1.3. Effect of air flow. The DTG curves of FLO-U for the different air flows are presented in Fig. 4-c. Increasing air flow resulted in increased DTG peak of the first degradation step (from 220 °C to 360 °C). Indeed, the maximum weight loss rate of the main degradation peak was higher as the air flow increased. At 800 °C, the residual mass increased slightly when the air flow increased. A higher flow rate increases the amount of air in the heating cell, which catalyses and accelerates the decomposition of the stem fragment components. Benítez-Guerrero et al. (2014) found the same trends for hot-washed sisal fibres.

3.1.1.4. Effect of sample amount. The DTG curves for samples of 5, 10 and 15 mg of FLO-U are presented in Fig. 4-d. As the total sample amount increased, the weight loss rate corresponding to the main degradation peak in DTG was more important. The acceleration of the degradation is most likely due to the heat transfer mechanism by convection within the heating cell. On one hand, the sample amount influences the height reached by the sample in the crucible, and therefore the flow pattern and velocity of the air around and within the crucible. For these reasons, the air flow around the sample increases as its amount increases, which increases in turns its degradation rate. On the other hand, the amount of sample in the crucible should also affect the thermal gradient within the sample that increases with the sample weight. As discussed above higher thermal gradient within the samples should lead to a decrease of the mass loss rate and a shift of the

Table 3
Sampling A. Thermal properties of miscanthus stem fragments from the upper and lower internodes of the different genotypes (FLO, GIGB, GOL, H5, MAL, SAC).

Genotypes / internodes	Stem region	Starting degradation temperature (°C)	DTG Peak 1 Temperature (°C)	DTG Peak 1 Value (-1.10^{-3} % s^{-1})	DTG Peak 2 Temperature (°C)	DTG Peak 2 Value (-1.10^{-3} % s^{-1})	Mass loss 180 − 360 °C (%)	Mass loss 360 − 500 °C (%)	Mass of residue at 800 °C (%)
FLO-U	Upper part	230	294	1.88	–	–	66.74	20.77	7.39
GIGB-U		223	292	2.00	–	–	67.47	18.05	6.31
GOL-U		230	295	1.39	317	1.95	66.77	8.06	5.91
H5-U		233	299	1.31	319	1.96	67.26	8.69	4.32
MAL-U		229	294	1.55	311	1.68	67.07	10.44	5.67
FLO-L	Lower part	230	293	1.34	–	–	63.69	10.47	5.92
GIGB-L		230	302	1.55	–	–	63.79	10.75	5.99
H5-L		231	301	1.29	317	1.38	63.31	11.06	3.76
SAC-L		240	297	1.18	321	2.04	64.32	7.82	6.00

degradation process to higher temperature due to heat and mass transfer limitations. In this study, the changes in the air flow pattern and velocity related to the amount and height of sample within the crucible appears to be predominant and to result in an increase of the mass loss rate with increasing sample weight.

Based on these experiments, all the following thermogravimetry analyses comparing stem fragments from upper and lower parts of different genotypes were performed under the same conditions: air at 50 mL/min from 25 °C to 400 °C at 10 °C/min and from 400 °C to 800 °C at 50 °C/min with a sample mass of 10 mg and a particle size comprised between 100 and 200 µm. Details about the ANOVA results for the effect of testing conditions are given in Table 3S in the supplemental file.

3.1.2. Influence of genotype, position along the stem and relation with biochemical composition

For the six different miscanthus genotypes, fragments from the upper and lower parts of the plant stems were analysed in order to evaluate the genotypic and fragment position effects on thermal stability. The starting degradation temperature, the first and second DTG peak temperatures, the mass losses and the mass of residue at 800 °C are reported in Table 3 for miscanthus stem fragments from upper and lower parts of the different genotypes. The relationship between the thermal stability and the biochemical composition of the different genotypes and stem regions is discussed below. Details about the ANOVA results for the effect of genotypes and position along the stem are given in Table 4S in the supplemental file.

3.1.2.1. Effect of genotype and position along the stem. Thermal gravimetry (TG) and DTG curves are presented for the upper and lower parts of the stems in Fig. 5 for FLO, GIGB and H5 genotypes. When considering the starting degradation temperature (Table 3), it was observed that the most thermally stable genotypes were H5 for the upper part with 233 °C and SAC for the lower part with 240 °C. In contrast, GIGB genotype started its degradation few degrees below, i.e. 230 °C and 233 °C for the upper and lower parts, respectively. No clear difference was observed when comparing upper and lower parts from a given genotype, the genotypic effect appearing as being the most significant factor (Table 4S).

The first degradation step from 180 °C to 360 °C took place following two kinds of behaviour depending on the genotype. The DTG curves of upper and lower parts of FLO and GIGB showed one peak whereas for the other genotypes, i.e. GOL, H5, MAL, SAC, the main peak presented a shoulder for both positions along the stem. This shoulder at 280 − 300 °C is often found when studying thermal degradation of plants (Jayaraman and Gökalp, 2015; Kim et al., 2014; Poletto et al., 2012). Jayaraman and Gökalp (2015) studied the degradation of miscanthus in various atmospheres. They suggest that the appearance of the shoulder on the first degradation peak is related to the presence of hemicelluloses in large amounts. On the other hand, when the concentration of hemicelluloses is low, its degradation is covered by the degradation of cellulose present in much higher concentration. In an oxidative atmosphere, pure cellulose degrades between 280 and 350 °C, with a maximum weight loss rate at 333 °C (Benítez-Guerrero et al., 2014). For miscanthus, cellulose degradation occurs at a slightly lower temperature and overlaps with the degradation of hemicellulose. This is due to the presence of large amounts of minerals in miscanthus (the weight of residue at 800 °C is 3.8–7.4% depending on the genotypes) which catalyse the cellulose degradation (Kim et al., 2014; Sivasangar et al., 2013). Therefore, a genotype effect is shown for thermal stability, the two genotypes of the *M. sacchariflorus* species (H5 and SAC) being the most thermally stable. A genotype effect is also observed for the number of peaks observed during the degradation. In contrast, the effect of the position along the stem appears non-significant.

3.1.2.2. Relation with biochemical composition. As discussed above, the

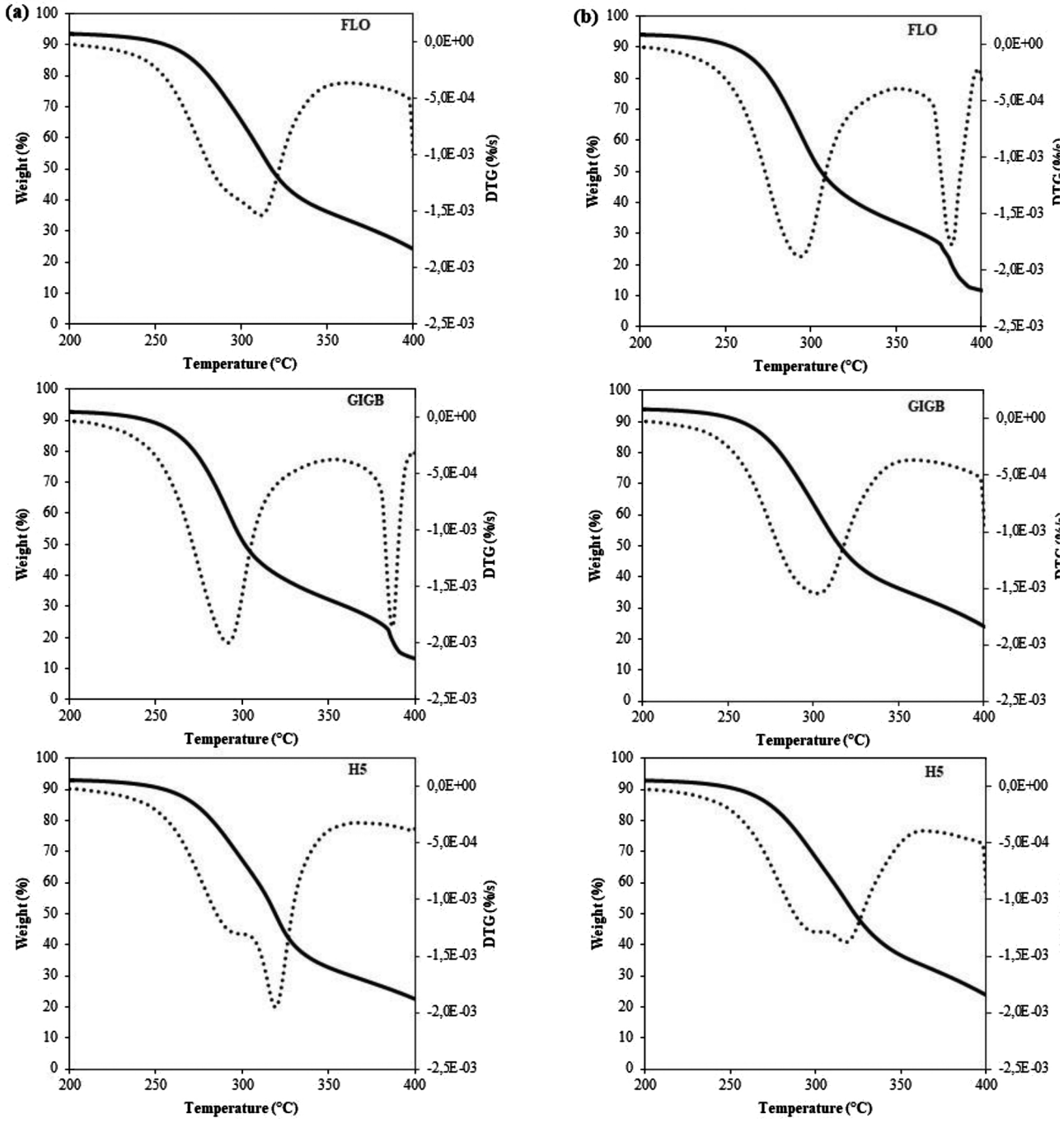

Fig. 5. Sampling A. Examples of TG (solid line) and DTG (dotted line) curves of the upper (a) and lower (b) parts for three genotypes FLO, GIGB and H5.

thermal stability of miscanthus stem fragments should be influenced by their biochemical composition, i.e. amounts of cellulosic and non-cellulosic constituents. The Pearson correlation coefficients between the different indicators of thermal stability (Table 3) and the biochemical composition (Table 1S) were calculated and highlighted some interesting linear dependences. As can be observed in Fig. 6, the starting degradation temperature cannot be significantly correlated to the biochemical composition, except for cellulose but with a low correlation coefficient of 0.4.

Regarding the other indicators of thermal stability, we can draw the following observations. The first DTG peak temperature, ranging from 292 °C to 302 °C, appeared to be negatively correlated to hemicelluloses content (r = -0.54) and positively correlated to lignin (r = 0.77) and p-coumaric (r = 0.69) contents. Less hemicellulose and more lignin and p-coumaric contents resulted in a shift of the first DTG peak at higher temperature. It is also interesting to note that higher amounts of hemicelluloses and ferulic acids were strongly correlated with an increase of the mass loss between 180 °C and 360 °C (r = 0.76 and 0.64, respectively), while the latter decreased with increasing amount of lignin (r = - 0.65). These results evidence the positive role of lignin and the negative role of hemicelluloses on thermal stability, in particular during the first degradation step of miscanthus stem fragments. High lignin content has been found to promote interactions between the different biomass components resulting in a delayed degradation and a broader DTG peak (Hosoya et al., 2007; Wang et al., 2011).

This set of data clearly shows the dependency of the thermal stability of miscanthus fragments towards non-cellulosic components, lignin increasing the thermal stability. Besides, the quantity of residue

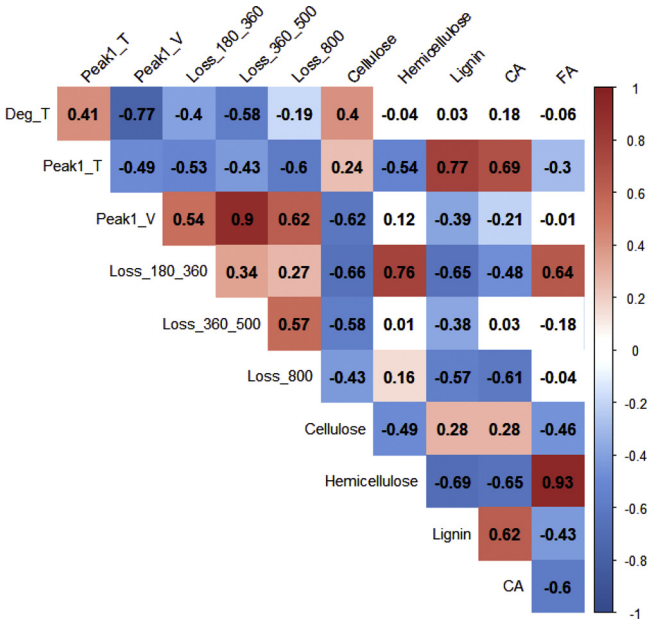

Fig. 6. Sampling A. Correlation coefficients *r* for the main thermal stability indicators of miscanthus stem fragments of each genotype and positions along the stem (upper and lower) in relation with the global biochemical composition measured on the corresponding miscanthus stem sections (Table1S). Notation correspondence with Tables 3 and 1S is as follows: Peak 1_T is DTG Peak 1 Temperature; Peak 1_V is DTG Peak 1 Value; Loss_180_360 is Mass loss 180-360 °C; Loss_360_500 is Mass loss 360-500 °C; Loss_800 is Mass of residue at 800 °C. CA is *p*-coumaric acid and FA is ferulic acid.

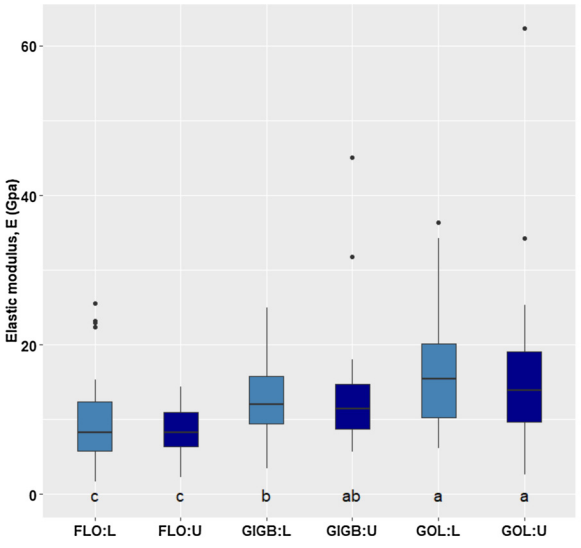

	Df Modulus	F value Modulus	Pr(>F) Modulus
Internode position	1	**22.3**	*
Genotype	2	**208.5**	*
Repetition	27	**104.8**	*
Internode position:Genotype	2	**49.7**	*
Residual	101		

Fig. 7. Sampling B. Top: boxplots of elastic modulus of the miscanthus stem fragments for upper (U) and lower (L) parts of FLO, GIGB, and GOL genotypes. Bottom: ANOVA results.

at 800 °C was found to be negatively correlated with most of the cellulosic and non-cellulosic components, which highlights the predominant role of the minerals on the ash content.

3.2. Dynamic mechanical characterization of miscanthus stem fragments

The dynamic mechanical characterization was performed using long and slender stem fragments from sampling B.

3.2.1. Elastic modulus of miscanthus stem fragments: effect of genotype and position along the stem

The elastic moduli of miscanthus stem fragments were determined by flexural vibration tests as described in Section 2.5, and results are presented in Fig. 7. In overall, the elastic moduli of stem fragments ranged from 8.2 GPa to 14.1 GPa depending on the genotype and position along the stem. These values are similar to the modulus of 10 GPa measured on stem fragments by nano-indentation by Bourmaud and Pimbert (2008). Of course, the moduli are much lower than the tensile modulus value of 55 GPa reported by Lundquist et al. (2003) for individual fibres extracted from miscanthus stems by a pulping process and mostly composed of cellulose originating from cell walls. Besides, these values are close to tensile moduli of other stem fragments as bamboo, 11 – 36 GPa (Bourmaud et al., 2018; Gurunathan et al., 2015). The ANOVA conducted on elastic modulus values revealed a marked genotype effect while there was no significant effect of the position along the stem (upper or lower parts) (Fig. 7). For both upper or lower parts, stem fragments of GOL genotype had the highest stiffness (14.1 GPa and 13.7 GPa for lower and upper parts, respectively) and stem fragments of FLO genotype the lowest (8.2 GPa and 8.3 GPa for lower and upper parts, respectively), GIGB stem fragments having intermediate stiffness (12.1 GPa and 10.6 GPa for lower and upper parts, respectively).

Kaack and his co-authors measured flexural elastic moduli on miscanthus stem sections of 10 cm, and found that lower parts exhibit higher stiffness (Kaack and Schwarz, 2001; Kaack et al., 2003). Other studies have shown that stem section moduli are higher for lower parts of sorghum (Esechie et al., 1977), oats (Norden and Frey, 1959) or wheat (O'Dogherty et al., 1995) stems, hence increasing their resistant to lodging. Besides, several studies dealt with the mechanical properties of plant fibres and their variation according to the position along the stem. It was reported for Agatha flax fibres with equivalent diameter that lower tensile elastic moduli and tensile strength are found for upper parts of flax stems, whereas flax fibres from the middle of the stem exhibited the highest mechanical properties and those from the lower part have intermediate ones (Charlet et al., 2009). Other studies on flax fibres have shown that fibres extracted from the lower parts have the lowest tensile stiffness and strength in the case of Hermès (Charlet et al., 2007) and Eden (Lefeuvre et al., 2015a) species. Fibres extracted from the middle part of the stem were found to have the highest mechanical properties in both studies. A study on woody hemp core reported lower flexural stiffness and strength for the lower positions along the stem as compared to the upper ones, woody hemp core from the middle internode having intermediate mechanical properties (Beaugrand et al., 2014). Tensile tests performed on sorghum fragments extracted from the bark revealed higher tensile strength and modulus in the middle region of the stem, followed by the upper positions and the lower positions (Bakeer et al., 2013). Based on all these published studies, it can be concluded that for many plants there is a clear dependency of the stiffness and strength of the tested sections, fragments or fibres according to their position along the stem. As reviewed in Table 4, it appears that stem sections are usually stiffer in the lower region of the stems (a characteristic linked to the role of this part of the stem, which is supporting the largest mechanical stresses) while fibres and stem fragments tend to be stiffer and more resistant in the middle and upper regions for several plants. It seems that there is no direct correlation between the stiffness of elementary fibres and stem fragments and the resulting stiffness of stem sections, i.e. stiffer elementary

Table 4
Literature review: mechanical properties of stem parts (the full stem is studied), stem fragments (stem is ground in small pieces) and elementary fibres extracted from the plant as a function of the position along the stem.

Sample types	Plants	Elastic modulus			Strength			References
		Position along stem			Position along stem			
		Lower	Middle	Upper	Lower	Middle	Upper	
Stem sections	Miscanthus	+		–				Kaack et al., 2003 Kaack and Schwarz, 2001
	Sorghum	+		–				Esechie et al., 1977
	Oats	+		–				Norden and Frey, 1959
	Wheat	+	+	–	+	+	–	O'Dogherty et al., 1995
Stem fragments	Hemp	–	+	+ +	–	+	+ +	Beaugrand et al., 2014
	Sorghum	–	+ +	+	–	+ +	+	Bakeer et al., 2013
Elementary fibres	Flax (Agatha)	+		–	+	+ +	–	Charlet et al., 2009
	Flax (Hermès)	–	+ +	+	–	+ +	+	Charlet et al., 2007
	Flax (Eden)	–	+ +	+	–	+ +	+	Lefeuvre et al., 2015a

fibres and stem fragments are not necessarily localized in the stiffest stem regions.

This review of literature thus shows that, beyond the biochemical composition and structural organization (thickening of the secondary cell walls, microfibrillar angle, crystallinity index I_c) within cell walls that strongly influence the stiffness of elementary fibres and stem fragments, the histological organization along the stem and across its diameter (distribution, type and number of vessels) also plays a key role in the resulting stiffness distribution along the plant stem (Bourmaud et al., 2015).

In Fig. 8, coefficients of correlation r were determined between the elastic moduli of miscanthus stem fragments and the global biochemical composition (Table 1S) measured on the corresponding stem sections (Sampling A). The strongest significant correlations with elastic moduli were found for the ferulic and *p*-coumaric acids contents with $r = 0.58$ and $r = -0.66$, respectively. Correlation with hemicelluloses content give low non-significant r values of 0.26. In contrast with the studies mentioned above, cellulose and lignin contents did not show any correlation with the elastic moduli of stem fragments.

Regarding the correlation between the elastic moduli and the contents of the two phenolic acids, the stem fragments originating from the upper and lower parts of the GOL genotype showed the highest ferulic acid content, the lowest *p*-coumaric acid content and the highest stiffness (Fig. 9a and b).

In contrast, the GIGB and FLO genotypes which had lower elastic moduli, presented lower ferulic content and higher *p*-coumaric acid content. Furthermore, the ratio ferulic acid / *p*-coumaric acid (Fig. 8) was positively and strongly correlated with the elastic moduli ($r = 0.64$), highlighting the antagonistic effect of these two phenolic acids on stiffness of stem fragments.

Moving now to the crystallinity index (Table 1) and local biochemical composition (Table 2S) determined on the corresponding stem fragments (Sampling B), the strongest correlations (Fig. 10) were positive for arabinose and xylose and negative for lignin. Remarkably, glucose content corresponding to cellulose showed no correlation with crystallinity index.

Summarizing our results, the correlation of the elastic moduli of miscanthus stem fragments with their corresponding global and local biochemical analyses revealed a strong dependency towards non-

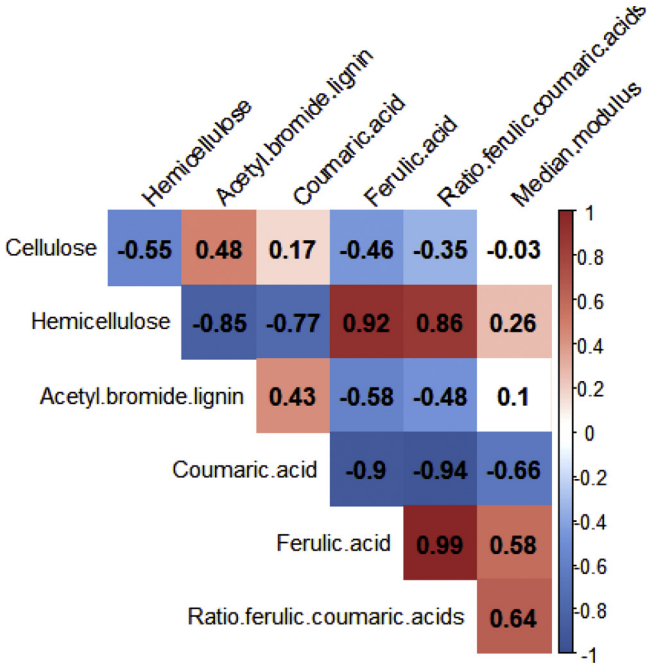

Fig. 8. Correlation coefficients r for the median elastic moduli of miscanthus stem fragments (Sampling B) for all genotype (FLO, GIGB and GOL) and positions along the stem (upper and lower) in relation with the global biochemical composition measured from Table 1S.

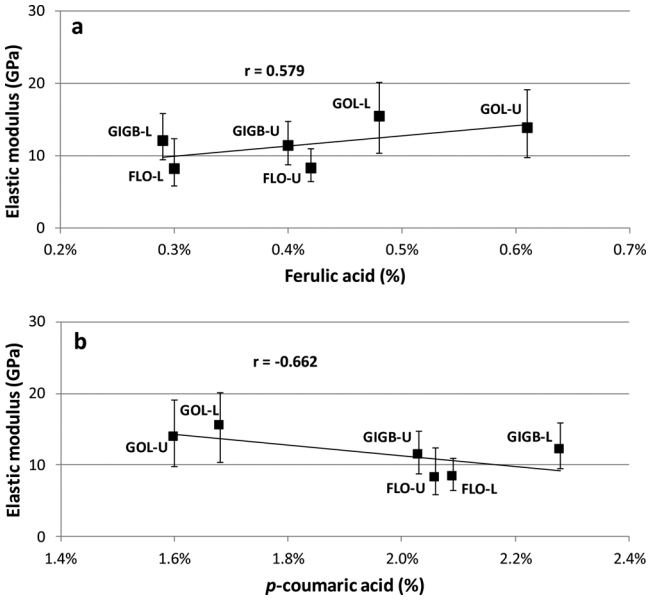

Fig. 9. Median and quartiles of the elastic moduli of miscanthus stem fragments (Sampling B) for each genotype (FLO, GIGB and GOL) and positions along the stem (upper and lower) as a function of ferulic acid (a) and *p*-coumaric acid (b) contents measured on the corresponding miscanthus stem sections (Table 1S).

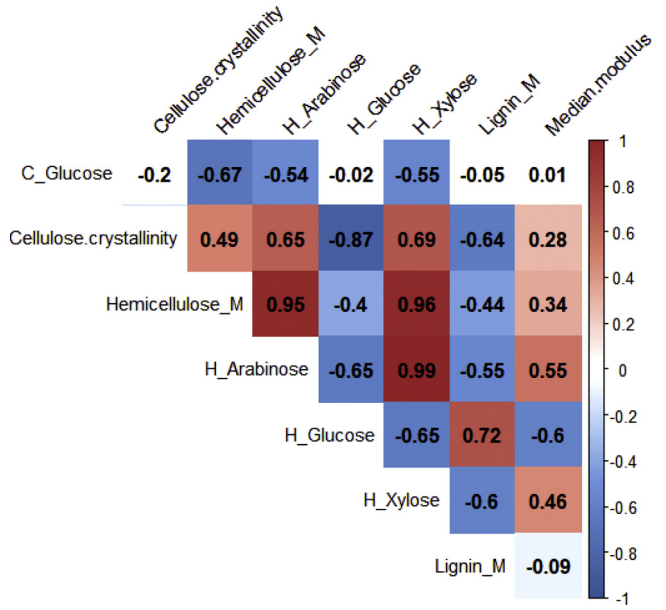

Fig. 10. Correlation coefficients *r* for the median elastic moduli of miscanthus stem fragments (Sampling B) for all genotype (FLO, GIGB and GOL) and positions along the stem (upper and lower) in relation with the crystallinity index (ground fraction sampling B) and the local biochemical composition (lignin, cellulose and hemicelluloses fractions) measured on the corresponding miscanthus stem fragments (Table 2S).

cellulosic components, especially the ratio ferulic / *p*-coumaric acids, and the hemicelluloses fraction. On the other hand, cellulose and lignin were poorly correlated with stem fragment moduli, a counter-intuitive result regarding its structural role. Studying the correlation between the biochemical composition of woody hemp core and their modulus measured by nanoindentation, Beaugrand et al. (2014) also found strong correlations with non-cellulosic components, i.e. arabinose, galactose and xylose (coefficient of determination R^2 of 0.80, 0.87 and 0.69, respectively). Furthermore, Antoine et al. (2003) found that arabinose was more prevalent in the stiffer and stronger tissue of wheat bran. It is known that non-cellulosic components are present within the cell walls but also in the intercellular regions, where they play a crucial role in the bonding of cellulose microfibrils and in the cohesion of plant cells. Ferulic acid is reported to be particularly abundant in grasses such as miscanthus (Molinari et al., 2013). It is also known to be covalently linked with arabinose substituents of arabinoxylans (hemicellulose) by ester bonds, acting as a universal connector between cell wall polymers (De Oliveira et al., 2015; Timpano et al., 2015). The *p*-coumaric acids are reported to be ester-linked to lignin units (Timpano et al., 2015). The cross-linking role of ferulic acid between pectic polysaccharides was supposed to have a major effect on the mechanical behaviour of cell walls in sugar beet (Waldron et al., 1997).

In contrast with published studies on elementary flax fibres in which the predominant role of the composition and structure of cell walls, especially the role of cellulose microfibrils, on the stress at rupture and stiffness was underlined, the present results show that in the case of miscanthus stem fragments, the stiffness is strongly dependent on non-cellulosic components. Our main finding is the strong correlation of elastic moduli of stem fragments with their ferulic and *p*-coumaric acids contents. Considering that these stem fragments are packed bundles of cells, the stress transfer mechanisms between the cells are expected to play an important role in their mechanical behaviour. In this regard, the intercellular non-cellulosic components implied in the cell cohesion should thus be considered as key structural constituents. Nevertheless, it should be noticed that elastic moduli of GIGB-L and GIGB-U stem fragments are significantly higher than those of FLO-L and FLO-U, while their global and local composition in non-cellulosic components are rather similar (Tables 1S and 2S). This highlights that the stiffness of miscanthus stem fragments cannot be simply related to the presence of one specific component. As pointed out by Charlet et al. (2009) and Lefeuvre et al. (2015b) for elementary flax fibres and Li et al. (2013) for hemp stalk fibres, the stiffness and strength of plant cells result from the complex biomolecular assemblies of cellulosic and non-cellulosic components and their organization within the cell walls. In particular, it is observed that GIGB-L and GIGB-U have slightly higher crystallinity indexes (Table 1) than FLO-L and FLO-U, which might be partly responsible for the higher stiffness measured for the GIGB genotype as compared to FLO.

3.2.2. Discussion on the interrelationships between genotypes, position along the stem, stem fragment dimensions and mechanical properties

Most of the materials studied in literature with data on the relation between biochemical composition, position along the stem and mechanical properties, are elementary fibres extracted from stems or other plant parts. This is vastly different from the lignocellulosic stem fragments studied here that are bundles of plant cells. In addition, in this study, two types of lignocellulosic fragments have been prepared: *(i)* first stem fragments originating from grounding and sieving procedure in selected ranges between a few microns to a few hundreds of microns long, and *(ii)* stem fragments selected because they have a long and slender shape, suitable for being tested mechanically. The latter slender stem fragments originate from the breaking of the stem through the propagation of cracks within and between the plant cells, and one can expect that they are not representative of the whole stem section from where they were extracted. Besides, although having been ground in the same conditions, stem fragments obtained for lower and upper parts of each genotype exhibit great variations in their dimensions and shapes (Fig. 11). Based on the measurement of their length L and minor diameter d_{min} (Section 2.5), their aspect ratio (L / d_{min}) was calculated and results are presented in Fig. 12.

For both positions along the stem, the ANOVA analysis revealed that the stem fragments extracted from the GOL genotype showed greater aspect ratios than FLO and GIGB (Fig. 12a). Besides, the aspect ratios of the respective lower and upper parts of GOL and GIGB genotypes were similar. In contrast, lower aspect ratios were obtained for the upper part of FLO genotype as compared to lower one. This trend suggests that the upper part of FLO stems tend to break into less elongated fragments during the grinding process. Note that upper positions of miscanthus stems were reported to contain more hemicelluloses than lower regions (Kaack et al., 2003). Biochemical analysis of FLO genotype (Table 1S) also revealed higher amounts of hemicelluloses and ferulic acid, and lower amounts of lignin and cellulose for upper parts. Considering that hemicelluloses and ferulic acid act as matrix and adhesive components in the middle lamellae between the cells, they could hinder the debonding of the plant cells upon grinding of upper parts. This may lead to different fragmentation processes, giving lower aspect ratios for FLO stem fragments from upper parts as compared to lower ones. Fragmentation processes are thus intimately related to the specific biochemical and structural characteristics of stem sections. This has an influence on the resulting dimensions of stem fragments (Figs. 11 and 12), and hence on the selection of stem fragment samples for mechanical characterization.

Based on these observations, the elastic modulus of each tested stem fragment was plotted as a function of its minor diameter and aspect ratio in Fig. 13a and b. It is found that the smaller diameters and the greater aspect ratios of stem fragments are related to higher elastic moduli. This tendency was valid for positions along the stem and genotypes except for FLO-U for which no trend was found. This relationship between the modulus and the diameter was also observed for flax fibres independent on the location of the extraction of fibres from the stem. Furthermore, higher strengths were obtained with thinner fibres, probably due to fewer defects within the fibre structure although these fibres are of different nature that the stem fragments considered

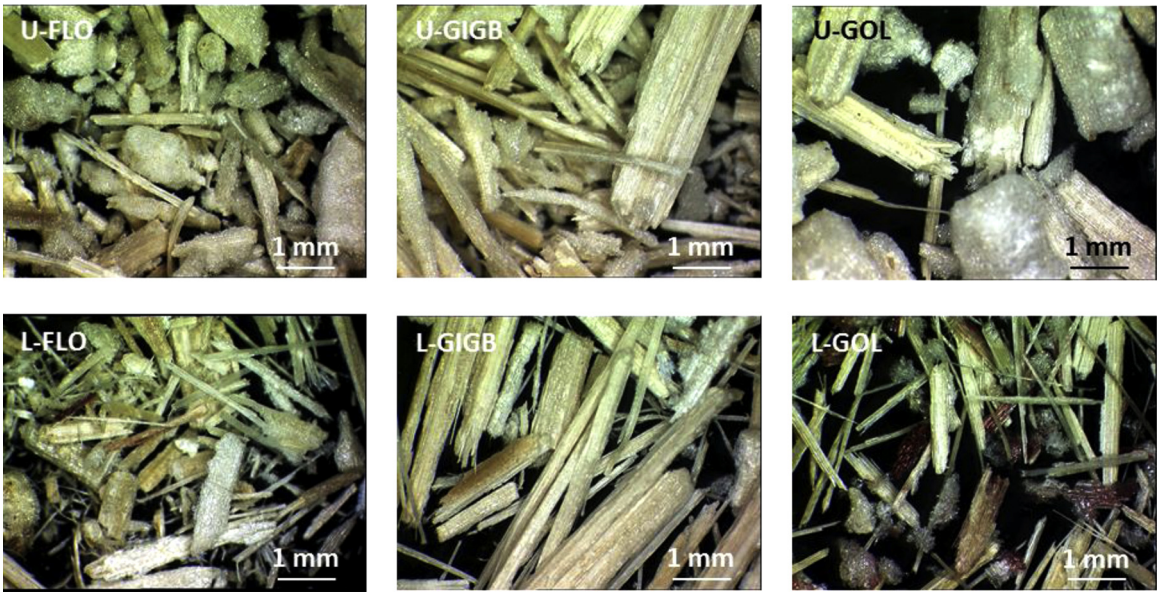

Fig. 11. Sampling B. Micrographs of ground fractions for upper (U) and lower (L) parts of FLO, GIGB and GOL genotypes.

here (Charlet et al., 2007).

Considering that the characteristics of genotypes and position along the stem can greatly influence the mechanical properties (Figs. 7–10) and the fragment sizes (Figs. 11 and 12), it can be assumed reciprocally that stem fragments with various sizes collected from the same genotype / position along the stem could also show variations in their chemical and structural features and hence in their mechanical properties. It is thus relevant to investigate the effect of genotype and position along the stem on the elastic modulus for defined diameter ranges of stem fragments. In Fig. 13c and d, moduli of the different genotypes and positions along the stem were plotted for two diameter ranges, i.e. 40–150 µm and 150–400 µm, 150 µm being the median diameter of all the stem fragments tested. Below 150 µm and based on ANOVA analysis, low variations of modulus were observed between genotypes and positions along the stem, except for upper parts of FLO which are significantly less rigid. Beyond 150 µm, modulus values were globally lower and less scattered. Lower parts of GIGB and GOL genotypes appeared to be stiffer.

These results demonstrated the difficulties to interpret the mechanical results as they are greatly influenced by the fragment shape and dimensions. Low diameters fragments show less variations between samples but also wide scattering in moduli. On the contrary, higher diameters fragments show lower scattering in moduli but more pronounced effects of the position along the stem level or genotype. Therefore, these data evidence that the measured stiffness of miscanthus stem fragments is greatly influenced by the fragment dimensions in relation with the genotypes and positions along the stem, their specific biochemical, structural and mechanical characteristics and their resulting behaviour upon grinding. Genotypic and position along the stem effects, fragmentation processes and mechanical properties of miscanthus stem fragments are thus strongly interconnected. When studying the mechanical behaviour of miscanthus stem fragments, and probably also for most lignocellulosic objects, it appears necessary to compare the results on restricted diameter ranges. This appears also essential for comparing genotypes.

4. Conclusions

The initial hypothesis of our work was that the miscanthus genotype effect on stem fragments and composite properties may be explained by biochemical characteristics. We also hypothesized that the composition of the stem is not homogeneous within the stem and may be variable between the genotypes. Using two different ways to select stem fragments from three to six genotypes and two positions along the stem, either by grinding-sieving or selecting manually long and slender fragments, the following results were obtained:

- Using the sieved fragments, the thermal analysis showed that the starting degradation temperature cannot be correlated to the biochemical composition. There was a slight dependency of the thermal stability of miscanthus fragments towards non-cellulosic components with the first DTG peak temperature being negatively correlated to hemicelluloses content and positively correlated to lignin and p-coumaric contents. There is a dependency of the thermal stability of miscanthus fragments towards non-cellulosic components, with the lignin content increasing the thermal stability.
- Using the long and slender fragments, it was shown that there is a clear effect of genotypes on the modulus while more limited effect of the position along the stem was detected. There was a noticeable correlation of elastic modulus with the xylose and arabinose contents and no correlation with crystallinity index, cellulose and lignin contents, this latter result being counter-intuitive regarding the important structural role of cellulose. In contrast, there was a strong correlation of elastic moduli with ferulic and *p*-coumaric acid contents, the ferulic acid / p-coumaric acid ratio being positively and strongly correlated with the elastic moduli. Besides, it was shown that size and shape of stem fragments can be related to genotypes and position along the stem. Fragmentation processes are thus intimately related to the specific biochemical and structural characteristics of stem sections: higher elastic moduli were found for smaller diameters and greater aspect ratios of fragments. The measured stiffness of miscanthus stem fragments is thus influenced by the fragment dimensions in relation with the genotypes and positions along the stem, their specific biochemical, structural and mechanical characteristics and their resulting behaviour upon grinding.

Our results highlight that genotypic and position along the stem effects, fragmentation processes and thermal and mechanical properties of miscanthus stem fragments are interconnected. Such detailed experiments and results on stem fragments are of interest for a reliable selection of genotypes that should give the best thermal and mechanical performances for polymer composites. They are also of interest for breeding in order to obtain better genotypes.

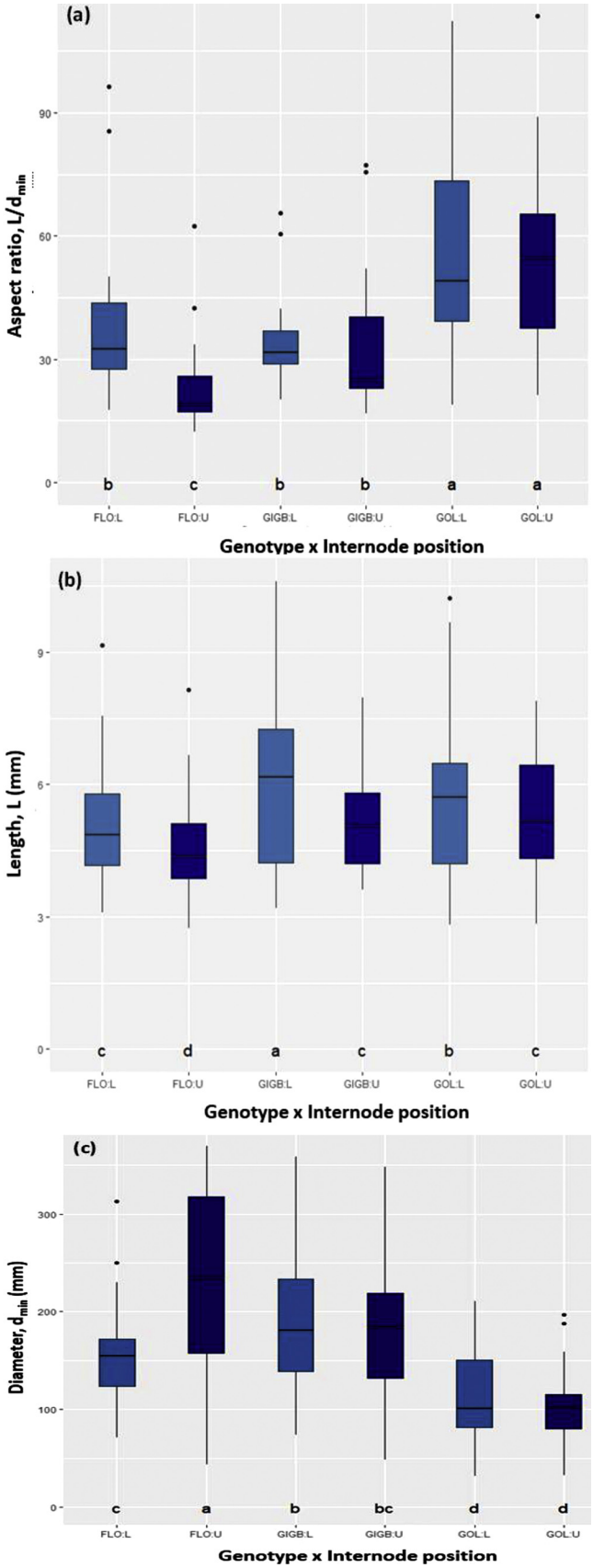

Fig. 12. Sampling B. Aspect ratio (a), length (b) and diameter (c) of the fragments selected for the mechanical characterization of lower (L) and upper (U) parts of FLO, GIGB, and GOL genotypes.

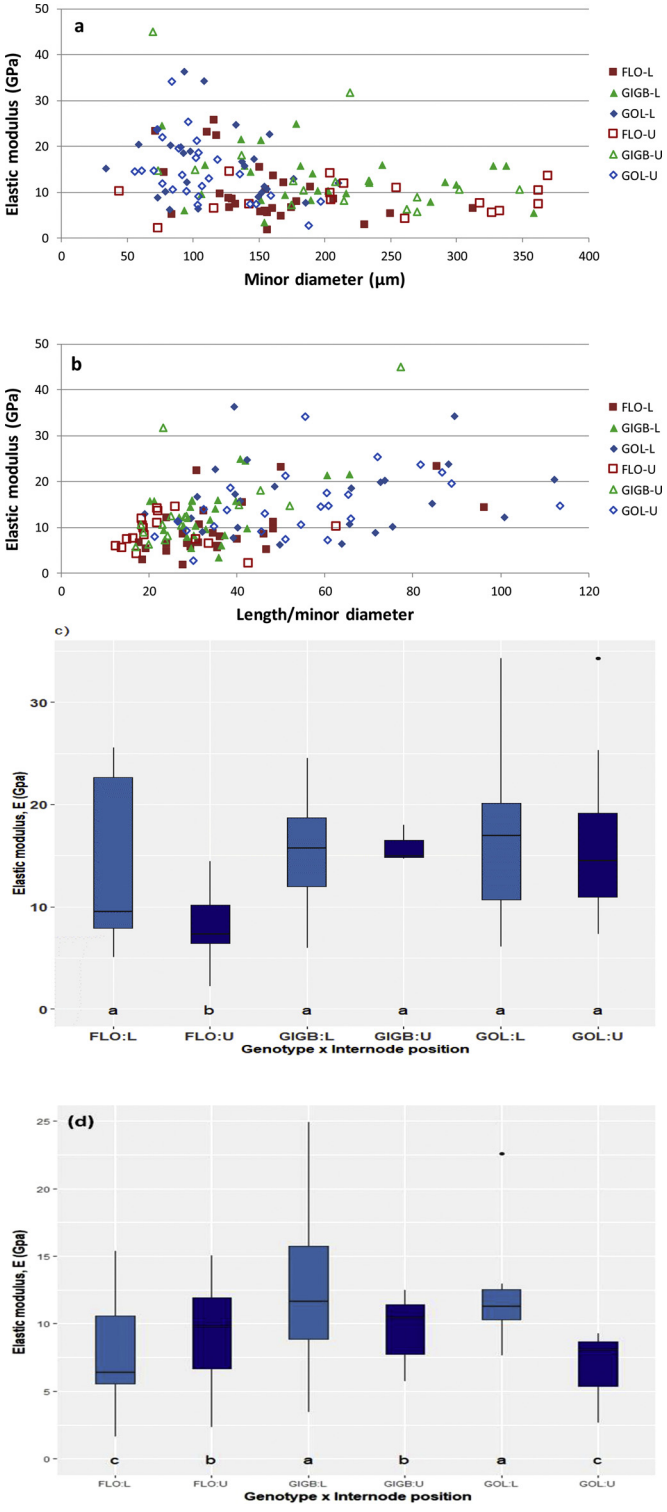

Fig. 13. Sampling B. Elastic modulus of miscanthus stem fragments as a function of the minor diameter (a) and the aspect ratio (b), and for restricted diameter range (c) 40 µm to 150 µm and (d) 150 µm to 400 µm according to upper (U) and lower (L) parts of FLO, GIGB, and GOL genotypes.

CRediT authorship contribution statement

Lucie Chupin: Writing - original draft. **Lata Soccalingame:** Writing - original draft. **Dieter de Ridder:** Investigation. **Emilie Gineau:** Investigation. **Grégory Mouille:** Investigation. **Stéphanie Arnoult:** Investigation. **Maryse Brancourt-Hulmel:** Writing - review & editing.

Catherine Lapierre: Writing - review & editing. **Luc Vincent:** Data curation. **Alice Mija:** Data curation. **Stéphane Corn:** Data curation. **Nicolas Le Moigne:** Writing - review & editing. **Patrick Navard:** Supervision, Writing - review & editing.

Declaration of Competing Interest

The authors report no declarations of interest.

Acknowledgements

This research work was supported by the Biomass For the Future project (funded by ANR-BTBR-006) and the BIOSORG project supported by the Agropolis (Labex Agro) and Cariplo foundations.

Appendix A. Supplementary data

Supplementary material related to this article can be found, in the online version, at doi:https://doi.org/10.1016/j.indcrop.2020.112863.

References

Alix, S., Goimard, J., Morvan, C., Baley, C., 2009. Influence of pectin structure on mechanical properties of flax fibres: a comparison between a linseed-winter variety (Oliver) and a fibres-spring variety of flax (Hermès). Pectins Pectinases, Ed. HA Sch. RGF Visser AGJ Voragen 87–96. .

Antoine, C., Peyron, S., Mabille, F., Lapierre, C., Bouchet, B., Abecassis, J., Rouau, X., 2003. Individual contribution of grain outer layers and their cell wall structure to the mechanical properties of wheat bran. J. Agric. Food Chem. 51 (7), 2026–2033. https://doi.org/10.1021/jf0261598.

Bakeer, B., Taha, I., El-Mously, H., Shehata, S.A., 2013. On the characterisation of structure and properties of sorghum stalks. Ain Shams Eng. J. 4, 265–271. https://doi.org/10.1016/j.asej.2012.08.001.

Barneto, A.G., Vila, C., Ariza, J., Vidal, T., 2011. Thermogravimetric measurement of amorphous cellulose content in flax fibre and flax pulp. Cellulose 18, 17–31. https://doi.org/10.1007/s10570-010-9472-0.

Beaugrand, J., Nottez, M., Konnerth, J., Bourmaud, A., 2014. Multi-scale analysis of the structure and mechanical performance of woody hemp core and the dependence on the sampling location. Ind. Crops Prod. 60, 193–204. https://doi.org/10.1016/j.indcrop.2014.06.019.

Benítez-Guerrero, M., López-Beceiro, J., Sánchez-Jiménez, P.E., Pascual-Cosp, J., 2014. Comparison of thermal behavior of natural and hot-washed sisal fibers based on their main components: cellulose, xylan and lignin. TG-FTIR analysis of volatile products. Thermochim. Acta 581, 70–86. https://doi.org/10.1016/j.tca.2014.02.013.

Bledzki, A.K., Gassan, J., 1999. Composites reinforced with cellulose based fibres. Prog. Polym. Sci. 24, 221–274. https://doi.org/10.1016/S0079-6700(98)00018-5.

Bok, J.P., Choi, H.S., Choi, J.W., Choi, Y.S., 2013. Fast pyrolysis of Miscanthus sinensis in fluidized bed reactors: characteristics of product yields and biocrude oil quality. Energy 60, 44–52. https://doi.org/10.1016/j.energy.2013.08.024.

Bourmaud, A., Pimbert, S., 2008. Investigations on mechanical properties of poly(propylene) and poly(lactic acid) reinforced by miscanthus fibers. Compos. Part A Appl. Sci. Manuf. 39, 1444–1454. https://doi.org/10.1016/j.compositesa.2008.05.023.

Bourmaud, A., Morvan, C., Bouali, A., Placet, V., Perré, P., Baley, C., 2013. Relationships between micro-fibrillar angle, mechanical properties and biochemical composition of flax fibers. Ind. Crops Prod. 44, 343–351. https://doi.org/10.1016/j.indcrop.2012.11.031.

Bourmaud, A., Gibaud, M., Lefeuvre, A., Morvan, C., Baley, C., 2015. Influence of the morphology characters of the stem on the lodging resistance of Marylin flax. Ind. Crops Prod. 66, 27–37. https://doi.org/10.1016/j.indcrop.2014.11.047.

Bourmaud, A., Beaugrand, J., Shah, D.U., Placet, V., Baley, C., 2018. Towards the design of high-performance plant fibre composites. Prog. Mater. Sci. 97, 347–408. https://doi.org/10.1016/j.pmatsci.2018.05.005.

Canché-Escamilla, G., Rodriguez-Laviada, J., Cauich-Cupul, J.I., Mendizábal, E., Puig, J.E., Herrera-Franco, P.J., 2002. Flexural, impact and compressive properties of a rigid-thermoplastic matrix/cellulose fiber reinforced composites. Compos. Part A Appl. Sci. Manuf. 33, 539–549. https://doi.org/10.1016/S1359-835X(01)00136-1.

Charlet, K., Baley, C., Morvan, C., Jernot, J.P., Gomina, M., Bréard, J., 2007. Characteristics of Hermès flax fibres as a function of their location in the stem and properties of the derived unidirectional composites. Compos. Part A Appl. Sci. Manuf. 38, 1912–1921. https://doi.org/10.1016/j.compositesa.2007.03.006.

Charlet, K., Jernot, J.P., Gomina, M., Bréard, J., Morvan, C., Baley, C., 2009. Influence of an Agatha flax fibre location in a stem on its mechanical, chemical and morphological properties. Compos. Sci. Technol. 69, 1399–1403. https://doi.org/10.1016/j.compscitech.2008.09.002.

Clifton-Brown, J., Chiang, Y.C., Hodkinson, T.R., 2008. Miscanthus genetic resources and breeding potential. In: Vermerris, W. (Ed.), Genetic Improvement of Bioenergy Crops. Springer Science, New York, pp. 273–290.

Clifton-Brown, J., et al., 2019. Breeding strategies to improve Miscanthus as a sustainable source of biomass for bioenergy and biorenewable products. Agronomy 9, 673–690. https://doi.org/10.3390/agronomy9110673.

Corn, S., Dupuy, J.-S., Ienny, P., Daridon, L., 2012. Vibration analysis techniques for detecting filler-matrix decohesion in composites. Revue des composites et des matériaux avancés 22 (1), 77–90. https://doi.org/10.3166/rcma.22.77-90.

Corn, S., Le Moigne, N., Jing, C., Voisin, G., Bergeret, A., 2013. A vibration-based NDT method for monitoring the stiffness of short natural fibres. In: The 5th International Conference on Structural Analysis of Advanced Materials. Kos, Greece.

Cortés, A.M., Bridgwater, A.V., 2015. Kinetic study of the pyrolysis of miscanthus and its acid hydrolysis residue by thermogravimetric analysis. Fuel Process. Technol. 138, 184–193. https://doi.org/10.1016/j.fuproc.2015.05.013.

Danalatos, N., Archontoulis, S., Mitsios, I., 2007. Potential growth and biomass productivity of Miscanthus × giganteus as affected by plant density and N-fertilization in central Greece. Biomass Bioenergy 31, 145–152. https://doi.org/10.1016/j.biombioe.2006.07.004.

De Oliveira, D.M., Finger-Teixeira, A., Rodrigues Mota, T., Salvador, V.H., Moreira-Vilar, F.C., Correa Molinari, H.B., Craig Mitchell, R.A., Marchiosi, R., Ferrarese-Filho, O., Dantas dos Santos, W., 2015. Ferulic acid: a key component in grass lignocellulose recalcitrance to hydrolysis. Plant Biotechnol. J. 13, 1224–1232. https://doi.org/10.1111/pbi.12292.

Deyholos, M.K., Potter, S., 2014. Engineering bast fibre feedstocks for use in composite materials. Biocatal. Agric. Biotechnol. 3, 53–57. https://doi.org/10.1016/j.bcab.2013.09.001.

Dhirhi, N., Shukla, R., Patel, N.B., Sahu, H., Mehta, N., 2015. Extraction method of flax fibre and its uses. Plant Archives 15, 711–716.

Dicker, M.P.M., Duckworth, P.F., Baker, A.B., Francois, G., Hazzard, M.K., Weaver, P.M., 2014. Green composites: A review of material attributes and complementary applications. Compos. A: Appl. Sci. Manuf. 56, 280–289. https://doi.org/10.1016/j.compositesa.2013.10.014.

Esechie, H.A., Maranville, J.W., Ross, W.M., 1977. Relationship of stalk Morphology and chemical composition to lodging resistance in sorghum. Crop Sci. 17, 609–612. https://doi.org/10.2135/cropsci1977.0011183X001700040032x.

Fukushima, R.S., Hatfield, R.D., 2001. Extraction and isolation of lignin for utilization as a standard to determine lignin concentration using the acetyl bromide spectrophotometric method. J. Agric. Food Chem. 49 (7), 3133–3139. https://doi.org/10.1021/jf010449r.

Giesche, H., 2006. Mercury porosimetry: a general (practical) overview. Part. Part. Syst. Charact. 23, 9–19. https://doi.org/10.1002/ppsc.20061009.

Girijappa, Y.G.T., Rangappa, S.M., Parameswaranpillai, J., Siengchin, S., 2019. Natural fibers as sustainable and renewable resource for development of eco-friendly composites: a comprehensive review. Front. Mater. 6https://doi.org/10.3389/fmats.2019.00226. Article 226.

Girones, J., Vo, L., Arnoult, S., Brancourt-Hulmel, M., Navard, P., 2016. Miscanthus stem fragment – reinforced polypropylene composites: development of an optimized preparation procedure at small scale and its validation for differentiating genotypes. Polym. Test. 55, 166–172. https://doi.org/10.1016/j.polymertesting.2016.08.023.

Gurunathan, T., Mohanty, S., Nayak, S.K., 2015. A review of the recent developments in biocomposites based on natural fibres and their application perspectives. Compos. Part A Appl. Sci. Manuf. 77, 1–25. https://doi.org/10.1016/j.compositesa.2015.06.007.

Harholt, J., Jensen, J.K., Sørensen, S.O., Orfila, C., Pauly, M., Scheller, H.V., 2006. ARABINAN DEFICIENT 1 is a putative arabinosyltransferase involved in biosynthesis of pectic arabinan in Arabidopsis. Plant Physiol. 140, 49–58. https://doi.org/10.1104/pp.105.072744.

Heo, H.S., Park, H.J., Yim, J.-H., Sohn, J.M., Park, J., Kim, S.-S., Ryu, C., Jeon, J.-K., Park, Y.-K., 2010. Influence of operation variables on fast pyrolysis of Miscanthus sinensis var. Purpurascens. Bioresour. Technol. 101, 3672–3677. https://doi.org/10.1016/j.biortech.2009.12.078.

Hermans, P.H., Weidinger, A., 1961. Relative intensities of the crystalline X-ray lines in cellulose fibres. Text. Res. J. 31, 558–571.

Hosoya, T., Kawamoto, H., Saka, S., 2007. Cellulose–hemicellulose and cellulose–lignin interactions in wood pyrolysis at gasification temperature. J. Anal. Appl. Pyrolysis 80, 118–125. https://doi.org/10.1016/j.jaap.2007.01.006.

Jayaraman, K., Gökalp, I., 2015. Pyrolysis, combustion and gasification characteristics of miscanthus and sewage sludge. Energy Convers. Manage. 89, 83–91. https://doi.org/10.1016/j.enconman.2014.09.058.

Johnson, M., Tucker, N., Barnes, S., Kirwan, K., 2005. Improvement of the impact performance of a starch based biopolymer via the incorporation of *Miscanthus giganteus* fibres. Ind. Crops Prod. 22, 175–186. https://doi.org/10.1016/j.indcrop.2005.08.004.

Kaack, K., Schwarz, K.-U., 2001. Morphological and mechanical properties of Miscanthus in relation with harvesting, lodging, and growth conditions. Ind. Crops Prod. 14, 145–154.

Kaack, K., Schwarz, K.-U., Brander, P.E., 2003. Variation in morphology, anatomy and chemistry of stems of Miscanthus genotypes differing in mechanical properties. Ind. Crops Prod. 17, 131–141. https://doi.org/10.1016/S0926669002000936.

Kim, J.-Y., Oh, S., Hwang, H., Moon, Y.-H., Choi, J.W., 2014. Assessment of miscanthus biomass (Miscanthus sacchariflorus) for conversion and utilization of bio-oil by fluidized bed type fast pyrolysis. Energy 76, 284–291. https://doi.org/10.1016/j.energy.2014.08.010.

Kong, E., Liu, D., Guo, X., Yang, W., Sun, J., Li, X., Zhan, K., Cui, D., Lin, J., Zhang, A., 2013. Anatomical and chemical characteristics associated with lodging resistance in wheat. Crop J. 1, 43–49. https://doi.org/10.1016/j.cj.2013.07.012.

Lefeuvre, A., Bourmaud, A., Baley, C., 2015a. Optimization of the mechanical performance of UD flax/epoxy composites by selection of fibres along the stem. Compos. Part A Appl. Sci. Manuf. 77, 204–208. https://doi.org/10.1016/j.compositesa.2015.07.009.

Lefeuvre, A., Le Duigou, A., Bourmaud, A., Kervoelen, A., Morvan, C., Baley, C., 2015b. Analysis of the role of the main constitutive polysaccharides in the flax fibre mechanical behaviour. Ind. Crops Prod. 76, 1039–1048. https://doi.org/10.1016/j.indcrop.2015.07.062.

Lewandowski, I., Scurlock, J.M.O., Lindvall, E., Christou, M., 2003. The development and current status of perennial rhizomatous grasses as energy crops in the US and Europe. Biomass Bioenergy 25, 335–361. https://doi.org/10.1016/S0961-9534(03)00030-8.

Li, X., Wang, S., Dua, G., Wu, Z., Meng, Y., 2013. Variation in physical and mechanical properties of hemp stalk fibers along height of stem. Ind. Crops Prod. 42, 344–348. https://doi.org/10.1016/j.indcrop.2012.05.043.

Lundquist, L., Arpin, G., Leterrier, Y., Berthold, F., Lindström, M., Manson, J.-A.E., 2003. Alkali-methanol-anthraquinone pulping of miscanthus x giganteus for thermoplastic composite reinforcement. J. Appl. Polym. Sci. 92, 2132–2143.

Mohanty, A.K., Misra, M., Drzal, L.T., 2005. Natural Fibers, Biopolymer and Biocomposites. CRC Press, Boca Raton.

Molinari, H.B., Pellny, T.K., Freeman, J., Shewry, P.R., Mitchell, R.A., 2013. Grass cell wall feruloylation: distribution of bound ferulate and candidate gene expression in Brachypodium distachyon. Front. Plant Sci. Mar 15 (4), 50. https://doi.org/10.3389/fpls.2013.00050.

Muthuraj, R., Misra, M., Mohanty, A.K., 2015. Injection molded sustainable biocomposites from poly(butylene succinate) bioplastic and perennial grass. ACS Sustainable Chem. Eng. 3, 2767–2776. https://doi.org/10.1021/acssuschemeng.5b00646.

Norden, A.J., Frey, K.J., 1959. Factors associated with lodging resistance in oats. Agron. J. 51, 335–338. https://doi.org/10.2134/agronj1959.00021962005100060009x.

O'Dogherty, M.J., Huber, J.A., Dyson, J., Marshall, C.J., 1995. A study of the physical and mechanical properties of wheat straw. J. Agric. Eng. Res. 62, 133–142. https://doi.org/10.1006/jaer.1995.1072.

Onuaguluchi, O., Banthia, N., 2016. Plant-based natural fibre reinforced cement composites: a review. Cement Concrete Comp. 68, 96–108. https://doi.org/10.1016/j.cemconcomp.2016.02.014.

Pickering, K., 2008. Properties and Performance of Natural-Fibre Composites. CRC, Woodhead Publisher Ltd, Cambridge (England).

Poletto, M., Zattera, A.J., Forte, M.M.C., Santana, R.M.C., 2012. Thermal decomposition of wood: influence of wood components and cellulose crystallite size. Bioresour. Technol. 109, 148–153. https://doi.org/10.1016/j.biortech.2011.11.122.

Ragoubi, M., George, B., Molina, S., Bienaimé, D., Merlin, A., Hiver, J.-M., Dahoun, A., 2012. Effect of corona discharge treatment on mechanical and thermal properties of composites based on miscanthus fibres and polylactic acid or polypropylene matrix. Composites Part A: Appl. Sci. Manuf. 43, 675–685. https://doi.org/10.1016/j.compositesa.2011.12.025.

Ramamoorthy, S.K., Skrifvars, M., Persson, A., 2015. Review of natural fibers used in biocomposites: plant, animal and regenerated Cellulose Fibers. Polym. Rev. Phila. Pa (Phila Pa) 55, 107–162. https://doi.org/10.1080/15583724.2014.971124.

Ruland, W., 1961. X-ray determination of crystallinity and diffuse disorder scattering. Acta Crystallogr. 14, 1180–1185. https://doi.org/10.1107/S0365110X61003429.

Sena Neto, A.R., Araujo, M.A.M., Barboza, R.M.P., Fonseca, A.S., Tonoli, G.H.D., Souza, F.V.D., Mattoso, L.H.C., Marconcini, J.M., 2015. Comparative study of 12 pineapple leaf fiber varieties for use as mechanical reinforcement in polymer composites. Ind. Crops Prod. 64, 68–78. https://doi.org/10.1016/j.indcrop.2014.10.042.

Shafizadeh, F., McGinnis, G.D., Philpot, C.W., 1972. Thermal degradation of xylan and related model compounds. Carbohydr. Res. 25, 23–33. https://doi.org/10.1016/S0008-6215(00)82742-1.

Shen, D.K., Gu, S., 2009. The mechanism for thermal decomposition of cellulose and its main products. Bioresour. Technol. 100, 6496–6504. https://doi.org/10.1016/j.biortech.2009.06.095.

Shen, D.K., Gu, S., Bridgwater, A.V., 2010. Study on the pyrolytic behaviour of xylan-based hemicellulose using TG–FTIR and Py–GC–FTIR. J. Anal. Appl. Pyrolysis 87, 199–206. https://doi.org/10.1016/j.jaap.2009.12.001.

Sibout, R., Le Bris, P., Legée, F., Cézard, L., Renault, H., Lapierre, C., 2016. Structural redesigning Arabidopsis lignins into Alkali-Soluble Lignins through the expression of p-Coumaroyl-CoA:monolignol transferase PMT. Plant Phys. 170 (3), 1358–1366. https://doi.org/10.1104/pp.15.01877.

Sivasangar, S., Taufiq-Yap, Y.H., Zainal, Z., Kitagawa, K., 2013. Thermal behavior of lignocellulosic materials under aerobic/anaerobic environments. Int. J. Hydrogen Energy 38, 16011–16019. https://doi.org/10.1016/j.ijhydene.2013.09.083.

Szabo, P., Varhegyi, G., Till, F., Faix, O., 1996. Thermogravimetric / mass spectrometric characterization of two energy crops, Arundo donax and Miscanthus sinensis. J. Anal. Appl. Pyrolysis 36, 179–190. https://doi.org/10.1016/0165-2370(96)00931-X.

Tejado, A., Peña, C., Labidi, J., Echeverria, J.M., Mondragon, I., 2007. Physico-chemical characterization of lignins from different sources for use in phenol-formaldehyde resin synthesis. Bioresour. Technol. 98, 1655–1663. https://doi.org/10.1016/j.biortech.2006.05.042.

Terinte, N., Ibbett, R., Schuster, K.C., 2011. Overview on native cellulose and microcrystalline cellulose I structure studied by x-ray diffraction (WAXD): comparison between measurement techniques. Lenzinger Berichte 89, 118–131.

Thakur, V.K., Thakur, M.K., Gupta, R.K., 2014. Review: raw natural Fiber–based polymer composites. Int. J. Polym. Anal. Charact. 19, 256–271. https://doi.org/10.1080/1023666X.2014.880016.

Timpano, H., Sibout, R., Devaux, M.-F., Alvarado, C., Looten, R., Falourd, X., Pontoire, B., Martin, M., Legée, F., Cézard, L., Lapierre, C., Badel, E., Citerne, S., Vernhettes, S., Höfte, H., Guillon, F., Gonneau, M., 2015. Brachypodium cell wall mutant with enhanced saccharification potential despite increased lignin content. Bioenerg. Res. 8, 53–67. https://doi.org/10.1007/s12155-014-9501-1.

Updegraff, D.M., 1969. Semimicro determination of cellulose inbiological materials. Anal. Biochem. 32, 420–424. https://doi.org/10.1016/S0003-2697(69)80009-6.

Vo, L., Navard, P., 2016. Treatments of plant biomass for cementitious building materials – a review. Constr. Build. Mater. 121, 161–176. https://doi.org/10.1016/j.conbuildmat.2016.05.125.

Vo, L., Girones, J., Beloli, C., Chupin, L., di Giuseppe, E., Clément-Vidal, A., Soutiras, A., Pot, D., Bastianelli, D., Bonal, L., Navard, P., 2017. Processing and properties of sorghum stem fragment-polyethylene composites. Indus. Crops & Prod. 107, 386–398. https://doi.org/10.1016/j.indcrop.2017.05.047.

Vonk, C.G., 1973. Computerization of Ruland's X-ray Method for determination of the crystallinity in polymers. J. Appl. Crystallogr. 6, 148–152. https://doi.org/10.1107/S0021889873008332.

Waldron, K.W., Ng, A., Parker, M.L., Parr, A.J., 1997. Ferulic acid dehydrodimers in the cell walls of beta vulgaris and their possible pole in texture. J. Sci. Food Agric. 74, 221–228. https://doi.org/10.1002/(SICI)1097-0010(199706)74:2<221::AID-JSFA792>3.0.CO;2-Q.

Wang, S., Guo, X., Wang, K., Luo, Z., 2011. Influence of the interaction of components on the pyrolysis behavior of biomass. J. Anal. Appl. Pyrolysis 91, 183–189.

Yan, L., Chouw, N., Jararaman, K., 2014. Flax fibre and its composites – a review. Composites: Part B.: Eng. 56, 296–317. https://doi.org/10.1016/j.compositesb.2013.08.0814.

Zhang, K., Misra, M., Mohanty, A.K., 2014a. Toughened sustainable green composites from poly(3-hydroxybutyrate-co-3-hydroxyvalerate) based ternary blends and miscanthus biofibers. ACS Sustainable Chem. Eng. 2, 2345–2354. https://doi.org/10.1021/sc500353v.

Zhang, K., Nagarajan, V., Zarrinbakhsh, N., Mohanty, A.K., Manjusri, M., 2014b. Co-injection molded new green composites from biodegradable polyesters and miscanthus fibers. Macromol. Mater. Eng. 299, 436–446. https://doi.org/10.1002/mame.201300189.